University of Stavanger

Faculty of Science and Technology

MASTER'S THESIS

Study program/Specialization: Petroleum Engineering	Spring semester, 2015 Open
Writer: Dori Yosef Kalai	…………… …………… (Writer's signature)
Faculty supervisor: Prof. Zhixin Yu External supervisor: Dr. Øyvind Borg	
Tittel på bacheloroppgaven: Tørr reformering av Metan: utvikling av katalysator og termodynamiske analyse. Thesis title: Dry reforming of methane: catalyst development and thermodynamic analysis	
Credits (ECTS): 60	
Key words: Dry reforming of Methane Supported metal catalyst Catalyst deactivation Thermodynamics Kinetic models Reaction mechanism	Pages: 87 Stavanger, 10/08/2015

1

ACKNOWLEDGMENT

_____

First and foremost, I would like thank my supervisor Professor Zhixin Yu for his support and dedication in leading me throughout this work.

The shift from my previous field of study into this fascinating field of chemical engineering is challenging and sometimes difficult. All of this has been made possible thanks to the devotion and expertise of Professor Zhixin Yu, who believes in me and invests his valuable time and energy to guide and direct me.

Many thanks also for the generous help from my colleagues in the Department of Petroleum Engineering and to the department management staff for providing me this opportunity.

Finally, many thanks to my family who has helped me through the transition and supported me along the way. Thanks to their patience and the space they provide me with, I am able to acquire valuable knowledge and to develop skills that will benefit my further PhD studies.

ABSTRACT

_____

With the concern of global warming resulted of greenhouse gases (GHG), continuous efforts have been devoted to address this issue by advanced chemical reaction technologies to convert the main GHG gas CO_2 into useful products. Among the proposed solutions, dry reforming of methane (DRM) for synthesis gas (syngas) production emerges as a promising technology compared to the industrially applied technologies for syngas production.

DRM refers to the chemical reaction of methane and carbon dioxide to form hydrogen and carbon monoxide which are designated as synthetic gas. Due to the relatively low hydrogen to carbon monoxide ratio, this process is attractive for the Fischer-Tropsch (F-T) process of the Gas-to-Liquid (GTL) Technologies.

The DRM utilizes CO_2 as an oxidant to react methane over heterogeneous catalyst and has important environmental implications because of the consumption of both CO_2 and CH_4, both significantly contributing to the greenhouse effect. Converting these gases into a valuable syngas will reduce the atmospheric emissions of CO_2 and CH_4. This thesis presents a comprehensive review of the catalyst design and preparation, catalytic activity and thermodynamics-kinetics analysis, and focuses on the catalyst deactivation which is the main concern of this process.

Heterogeneous catalyst for DRM generally consists of active species dispersed on mesoporous supports coupled with a promoter. Literature reports that group VIII metals onto oxides supports are effective for this catalytic process. Although noble metals demonstrate highest catalytic stability, the bimetallic Ni-based catalysts appears to be promising for future processes in industrial scale. Furthermore, mesoporous supports play an important role in both catalytic activity enhancement and coke deposition prevention. It is accepted that the Al_2O_3 and TiO_2 supports are more promising, contribute to the enhanced catalytic activity and to the coke deposition prevention. In addition, promoters are non-active additives that improve the metallic dispersion over the support. Among the various reported promoters, Ce and ZrO_2 show remarkable performance of minimizing carbon deposition and preventing active metal sintering. In this work, special attention is also paid to the investigation of catalysts design and synthesis. despite the fact that the catalyst preparation methodology is already well defined, the realization to obtain the exact structure, morphology and function of the produced catalyst is still hard to achieve and drives the further investigation on more controllable preparation and characterization methods.

Finally, studies on thermodynamic and kinetics of DRM is also elaborated. The thermodynamic equilibrium analysis is based on Gibbs energy minimization method and are interconnected to the kinetic reaction mechanisms. Thermodynamic variable optimization is not fully identified yet and play an important role for gaining high DRM efficiency. In general, the DRM is favored

with low pressures of 1 bar, temperature range of 770-1170 °K and reactant (CO_2+CH_4) ratio close to unity.

DRM is a relatively simple reaction however its mechanism is difficult to predict and catalyst deactivation is still a great concern. Further systematic studies need to be done in order to achieve significant process improvement for the utilization of the DRM in large industrial scales.

TABLE OF CONTENTS

1   BACKGROUND

1.1   Greenhouse Gases, CO_2 Emission and Climate Change

Greenhouse gases (GHG) in the atmosphere are proposed to cause an increase in surface temperature of the globe, which is known as the greenhouse effect. The GHG include carbon dioxide (CO_2), methane (CH_4), oxides of nitrogen (N_2O), and fluorinated gases (F-gases). Observing the GHG distribution in the atmosphere (Figure 1) shows that the CO_2 and CH_4 are the two most abundant gases.
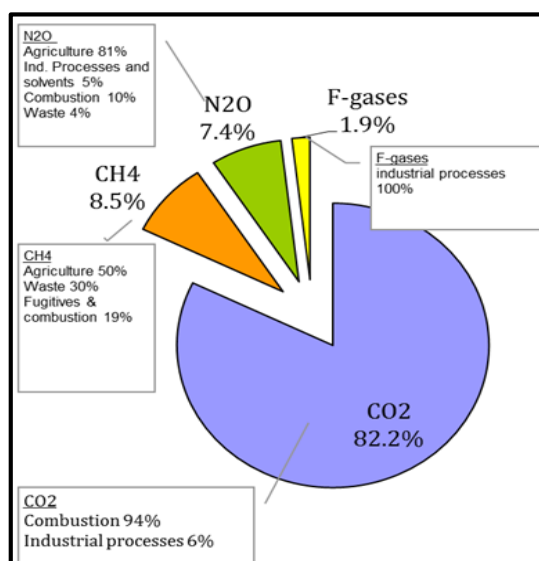
Fig. 1. Total GHG emissions by gas in EU-27, 2013. Source: United Nations Framework Convention on Climate Change (UNFCCC), May 2013.

GHG gas emissions are strongly related to the world population growth and consequently to the growing energy demand, evidenced by the fact that CH_4 and CO_2 emissions are resulted from the developing agriculture, natural gas process activities and fossil fuel combustions. Accordingly, the world's developed countries are leading campaigns to reduce the resulted GHG emissions. On March 2007 the European Council made a commitment to reduce GHG by at least 20% until 2020 compared to 1990 [1] with a net GHG reduction of 368 million tons of CO_2 per year. The Europe 2020 Strategy adopted on June 2010 (replacing the Lisbon Strategy) [1, 2] represents the current roadmap of the European Union for economic renewal with a goal to eventually decrease 30% GHG emissions by 2020.

1.2 CO_2 Capture and Storage

To overcome the above mentioned issues, multiple solutions have been proposed among which the carbon capture and storage and CO_2 utilization stand out as prominent alternatives. Carbon

capture and storage (CCS), which is sometimes called carbon capture and sequestration, prevents large amounts of CO_2 from being released into the atmosphere. The technology involves capturing CO_2 produced by large industrial plants or recovered CO_2 from natural gas fields, compressing it for transportation and then injecting it deep into a rock formation at a carefully selected and safe site, where it is permanently stored.

The Sleipner gas field produces over one million tons of pure CO_2 per year, which is injected into a deep saline aquifer below the North Sea (Figure 2). The Sleipner CCS plant is a key demonstration site for Carbon capture and storage (CCS) technology in Europe [3].
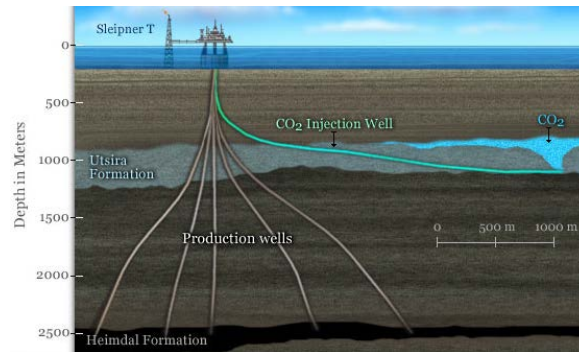
Fig. 2. Schematic cross section through the Sleipner CO_2 injection facility, where 1 million tons of pure CO_2 per year is injected below the North Sea.

The Natuna "D-Alpha" gas field, one of the major natural gas reserve in Indonesia with more than 200 TCF (Trillion cubic feet), is composed of 71% CO_2. The current plans for the development of this field include capture of 90% of the CO_2 and injection into two neighboring deep saline reservoirs 900 m beneath the Natuna sea bed (figure 3) [4]. The decision to employ CCS in this project is related to the produced CO_2 volume, which would create a massive point source equal to 0.5% of the current global emissions from fossil fuels if directly released to the atmosphere. However, if the CO_2 is stored in deep geological formations, then storage security largely depends on the integrity of the primary storage site. When combining the high geothermal gradient and the low hydrostatic pressure, the CO_2 becomes less dense and less viscous and ascend at an accelerating rate through the sediment column. In the event of primary leakage, escape of CO_2 to the ocean is inevitable and release of CO_2 to the atmosphere likely to occur [5, 6].

CCS (carbon capture and storage) provides a relatively cost-effective emission reduction, but has critical limitations: high capital investment costs, uncertain storage capacity, increasing public resistance to CCS and intensive energy consumption processes [7].
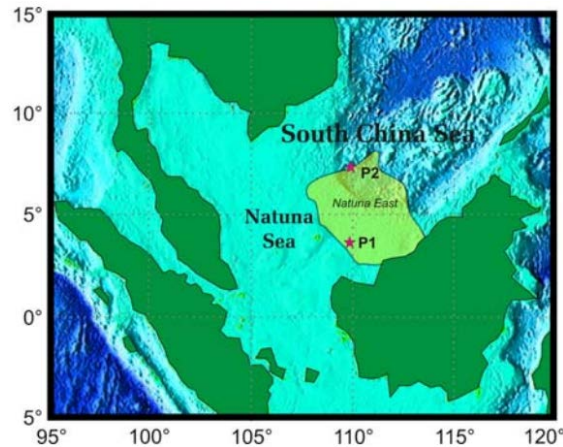
Fig. 3. Two optional points P1 (water depth 84 m) and P2 (water depth 1400 m) for the injection of 90% of the produced CO_2 in the Natuna "D-Alpha" gas field.

1.3 CO_2 Utilization: Conversion into Fuels and Chemicals

Rather than treating CO_2 as a waste and storing it underground, it can be regarded as a chemical feedstock for the upscaling synthesis that does not rely on a petrochemical source. CCU (carbon capture and utilization) process can rely on current post-combustion CCS technologies to provide added value products that can offset the costs of plant investment or even make the process profitable. The developing CCU technologies aim to convert CO_2 into gasoline, diesel fuel, jet fuel, and industrial chemicals in an economical and practical way. Currently, pilot scale CCU technologies only take a slipstream from the main flue gas supply but have the potential and economic viability to be scaled-up. The economic potential of CCU is limited by scale, however, some options can be attractive to pursue. Mainland Europe (in particular Germany), the US and Australia are well advanced in research and development of CCU technologies. Substantial investment has been made in those countries by extending CCS technology to incorporate CO_2 utilization in addition to storage [7].

This thesis will focus on one of the utilization options, *i.e.,* utilizing CO_2 as the raw material for the reforming of CH_4 for the production of valuable syngas, instead of treating it as a waste.

9

2   OVERVIEW OF REFORMING TECHNOLOGIES

2.1   Synthesis Gas Production

Synthesis gas (or syngas) is a mixture of H_2 and CO that is used for the production of a large number of chemical products and fuels such as ammonia, H_2 for refineries, diesel and methanol (Gas To Liquid technology, GTL) [9-13].

Motivated by the needs of alternatives sources for the chemical and petrochemical industries, Fischer and Tropsch initiated the dry (CO_2) methane reforming (DRM) studies over various metals for the synthesis of long-chain hydrocarbons back in 1928 [14]. However, the DRM process is currently not applied in industrial scales whereas the steam methane reforming (SMR, Eq. 2) is the principal process for the production of syngas from natural gas [15, 16].

Although SMR is utilized in the industry for decades, it still abstains drawbacks that motivate the development of other alternative reforming technologies:

A.   SMR Syngas is produced with a H_2/CO ratio ~ 3:1 that is higher than the needed ratio for the F-T synthesis of high value products.

B.   The endothermic SMR requires large amounts of heat supply which leads to high process cost.

C.   Operational costs and energy consumption are increased when excessive steam is used at a H_2O/CH_4 ratio of 3/4 for the inhibition of catalysts deactivation [3].

Together with the SMR, the partial oxidation, autothermal reforming, and more recently dry reforming and tri reforming are also being explored and utilized for syngas productions with various CO/H_2 ratios while all four processes suffer from the same deactivation mechanisms and high process costs [13]. In all cases the process uses an oxidizing agent to oxidize methane over heterogeneous catalyst and to produce CO and H_2 in a ratio that depends on the type of oxidant used. However, when pure H_2 is required, the methane decomposition is considered as a better process free of CO or CO_2, reducing the emission of CO_2 to as low as only 5% the volume of produced H_2 [5].

Dry Methane Reforming	$CH_4 + CO_2 \leftrightarrow 2CO + 2H_2$	$\Delta H^0_{298K}= 247 \ kJ \cdot mol^{-1}$	(1)

Steam Methane Reforming	$CH4 + H2O \leftrightarrow CO + 3H2$	$\Delta H0298K = 206 \ kJ \cdot mol\text{-}1$	(2)
Partial Oxidation	$CH_4 + 0.5O_2 \leftrightarrow CO + 2H_2$	$\Delta H^0_{298K} = -32 \ kJ \cdot mol^{-1}$	(3)
	$CH_4 + 2O_2 \leftrightarrow CO_2 + 2H_2O$	$\Delta H^0_{298K} = -802 \ kJ \cdot mol^{-1}$	(4)
Autothermal Reforming	$CH_4 + CO_2 \leftrightarrow 2CO + 2H_2$	$\Delta H^0_{298K} = 247 \ kJ \cdot mol^{-1}$	(1)
	$CH_4 + H_2O \leftrightarrow CO + 3H_2$	$\Delta H^0_{298K} = 206 \ kJ \cdot mol^{-1}$	(2)
Methane Decomposition (Methane Cracking)	$CH_4 \leftrightarrow C + 2H_2$	$\Delta H^0_{298K} = 75 \ kJ \cdot mol^{-1}$	(5)
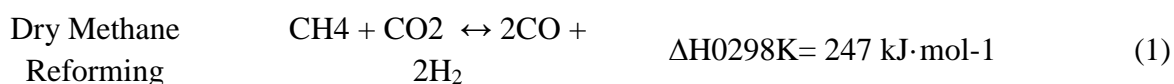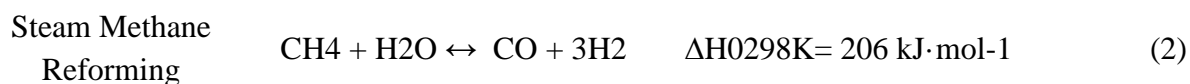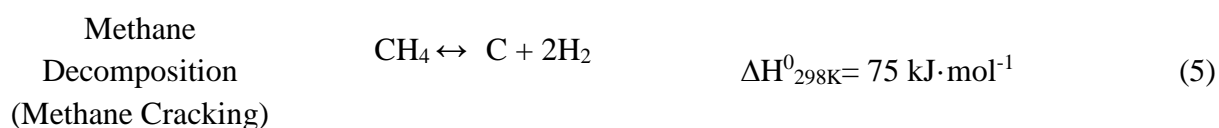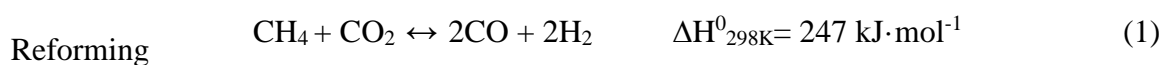
Reforming methods are basically divided into, *the endothermic methods* (DRM Eq. 1 and SMR Eq. 2) that demand high energy supplies to attain the activation energy and *the exothermic methods* (e.g., POM Eq. 3) which don't require heat supply. However, using pure oxygen brings a couple of technical and economic problems so that the industrial scale systems usually utilizes a mixture of oxygen, steam and/or CO_2 with methane. The ATR is reforming technology that aims at self-sustainable in terms of heat supply due to the existence of both endothermic and exothermic reactions.

The SMR generally involves processes that are comparable to the ATR although in SMR the oxidizing agent is H_2O (steam). The SMR energy balance is different from ATR since the production of steam itself requires an energy investment. Furthermore, the thermodynamics related to SMR are similar to the DRM but significantly different from an oxygen-based oxidation process. The SMR process is considered as the most mature technology for CH_4 reforming while the continuous studies of DRM aim to develop a process which is more sustainable and mitigates the rising CO_2 global problem.

In order to reduce activation energy, the reforming processes incorporate supported heterogeneous metallic catalyst that is specially designed and manufactured to inhibit catalysts deactivation. Deactivation occurs due to active sites coking, oxidation and/or sintering processes resulted by indirect reactions and process thermodynamics (mainly high temperatures effect). Generally, the catalysts are composed of various types of metals. In certain cases catalyst promoters are used for better dispersion of the active metal onto mesoporous surface of the support.

2.2   Steam Reforming of Methane

SMR is a mature reforming process that involves a reaction between natural gas (or other light hydrocarbons) and steam, normally carried out with catalyst at 1000–1273°K and 14–20 bar over a nickel-based catalyst [17]. A typical industrial steam reformer contains an array of catalyst-filled tubes suspended in a furnace, supplying the heat for the highly endothermic reforming reaction.

A typical SMR process (Figure 4) is divided into three main reversible process (i) Reforming, (ii) Shift and (iii) CO_2 Removal. The first reforming steps (Eq. 2 and 6) catalytically reacts methane with H_2O (steam) fed in the reformer furnace, to form H_2 and CO.

$$CH_4 + 2H_2O \leftrightarrow CO_2 + 4H_2 \qquad \Delta H^0_{298K} = 163 \text{ kJ·mol}^{-1} \qquad (6)$$

Due to the fact that this reforming reaction is highly endothermic, large amount of heat is provided by feeding supplemental natural gas to the furnace.

Fig. 4. : Flowsheet for a conventional SMR process [17].
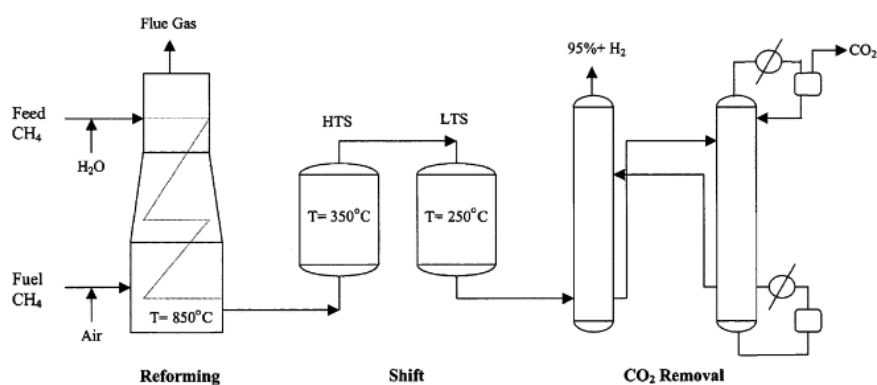
The effluent gas from the reformer contains about 76% H_2 (mol%), 13% CH_4, 12% CO and 10% CO_2 on a dry basis [17]. However, an excess of water supply leads to a more complete oxidation of carbon and production of higher hydrogen proportion. While usually the SMR leads to syngas with a H_2/CO ratio of 3 (Eq. 2), H_2/CO ratio of 2 (higher than the ideal) is

necessary for further conversion to synthetic fuels such as gasoline and diesel by F-T process [18, 19].

The reformer products are fed to a water gas shift (WGS) reactor where the reverse shift reaction (RSR, moderately exothermic and favored by low temperatures, Eq. 7) occurs. Therefore, when considering an operative high temperature above 750 °C for a substantial reforming conversion of CH_4, the produced gas is characterized by a 8–10% CO content on a dry basis [17]. In order to reduce CO content at the outlet of the SMR reactor, the produced syngas is conventionally fed to WGS reactor where the temperature is kept as low as 573–673 °K to favor the WGS reaction. If high purity H_2 is desired (up to 99%), normally either pressure swing adsorption (PSA) technology or amine scrubbing is used downstream to remove CO_2 [17].

$$CO + H_2O \leftrightarrow CO_2 + H_2 \qquad \Delta H^0_{298K} = -41 \text{ kJ·mol}^{-1} \qquad (7)$$

Similarly, industrial SMR catalysts are mostly based on Ni and face similar catalyst deactivation due to various kinds of carbonaceous deposits (coke) formed in the reactor [19]. Thermal stability of the catalysts is important, particularly since the Tammann temperature, above which Ni sintering can be expected, is less than the normal operating temperatures for steam reforming [20, 21]. Furthermore, the use of catalyst support also provides the high surface area and improves catalyst thermal stability. A support with high basicity promotes the reaction between the steam and the carbon which reduces the coke deposition.

Compared to DRM, autothermal and partial oxidation processes, the SMR is more developed and economic, and currently leading the industrial production of syngas or hydrogen.

2.3 Partial Oxidation of Methane

POM (Eq. 3) is a heterogeneous catalytic process, producing syngas with a H_2/CO ratio of 2:1, within a temperature range of 1270-1770°K and a wide pressure range of 1-80 bar [22, 23]. The indirect mechanisms of the partial oxidation consist of CH_4 combustion, DRM and SRM Eq. 8 ,1 and 2 respectively [24].

$$\text{Partial Oxidation} \qquad CH_4 + 0.5O_2 \leftrightarrow CO + 2H_2 \qquad \Delta H^0_{298K} = -32 \text{ kJ·mol}^{-1} \qquad (3)$$

$$\text{Methane Combustion} \qquad CH_4 + 2O_2 \leftrightarrow CO_2 + 2H_2O \qquad \Delta H^0_{298K} = -802 \text{ kJ·mol}^{-1} \qquad (8)$$
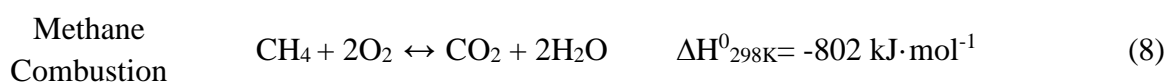
The POM occurs in two stages. In the first stage, methane is converted to CO_2 and H_2O until complete conversion of oxygen is achieved (oxygen is the limiting reactant at a stoichiometric feed ratio). In the second stage, syngas is produced via secondary DRM and SMR reactions.

Unlike DRM and SMR, non-catalytic homogeneous POM for synthesis gas production is industrially feasible. In Sarawak Malaysia, Shell successfully operates a highly selective non-catalytic process for production of synthesis gas at high temperatures, typically over 1400 °K and pressures of 50–70 bar. This process is part of the middle distillate synthesis process (SMDS) [25]. The use of a catalyst could significantly reduce the operating temperature required for the reaction, making the process less thermally complicated, however, more work is required to solve the catalyst deactivation problems.

The POM process presents thermodynamic advantages over SRM:

I.   Partial oxidation is mildly exothermic, while steam reforming is highly endothermic. Thus, a partial oxidation reactor would be more economical to heat. In addition, it can be combined with the endothermic reactions (SMR or DRM) to make these processes more energy efficient.
II.   The H_2/CO ratio produced in stoichiometric partial oxidation is ~ 2 and thus is ideal for downstream F-T processes, in particular for methanol synthesis. This fact avoids the need to remove valuable H_2, which is produced in excess in SMR.
III. The product gases from POM can be extremely low in CO_2 content, which often has to be removed before synthesis gas can be used.
IV.   POM technology avoids the need for large amounts of expensive superheated steam. However, an oxygen separation plant, which is also expensive, may be required in cases where the remained N_2 (from air) is undesirable in high-pressure downstream processes.

The high pressure and pure oxygen required by the economics of the downstream processes lead to high primary costs while further costs are expected for post treatments, separation of CO_2, and treatment of coke and soot. Further engineering studies and economic evaluation are needed in order to make this process more affordable and industry favored.

2.4   Autothermal Reforming

ATR is a heterogeneous catalytic process of combining the endothermic SMR or DRM with the exothermic oxidation process and its thermodynamics based on the optimal temperatures of the DRM [26]. The addition of O_2 to the reformed CH_4 is an effective method for heat supplying to the endothermic reaction, thus, there is less or no additional heat input.

Among all other reforming methods [26], the ATR, has been considered to be promising way due to its high efficiency, simplicity, more controllable H_2/CO ratio and easier process start-up [16] .

The ATR is usually carried out in two separate reaction zones in fixed bed reactor, as shown in Figure 5 and table 1 [27]. In the First Combustion Zone, CH_4 with pressure above 43 bar is preheated to 815 °K through combustion by O_2 into CO_2 and H_2O. The mixture gains the heat for the second zone and ensures the complete conversion of oxygen in feed, producing a hot stream with temperatures above 1573 °K [28]. In the second zone (Eq. 10), the thermal and catalytic zone, unconverted CH_4 is reformed by CO_2 and H_2O (steam). The main disadvantage of this technology is that the hot stream accelerates the thermal sintering and deactivation of the supported catalyst [28].
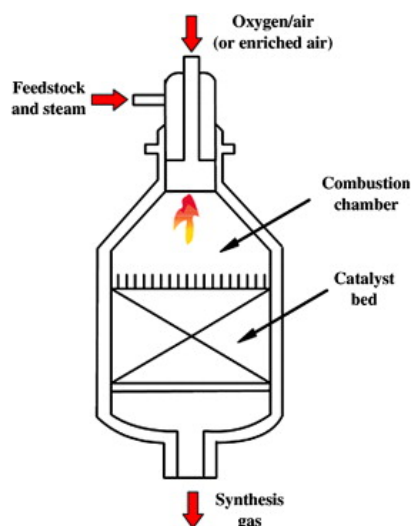
Fig. 5. Diagram of an ATR reactor.

Table 1: ATR reaction zones.

Reaction	Process Designation	Reaction number
POM	First combustion Zone	
SMR	Second Thermal and catalytic zone	
$CH_4+XCO_2+(1-X)/2O_2 \leftrightarrow (1+X)CO+2H_2$ $\Delta H^0_{298K} =(285X-38)$ kJ·mol^{-1} $0<X<1$	Second Thermal and catalytic zone	(10)

Autothermal reforming presents a flexible choice, providing reasonable H_2 and CO yields. Effectively, an ATR combines the exothermic nature of a POM reaction (hydrocarbon fuel

reacting with air) with the endothermic SMR to balance the heat requirements. Reactions can occur on the same catalyst or on a SMR catalyst located in proximity to the POM catalysts. The quality of the ATR reformate, defined in terms of H_2 mole fraction, is thus superior to the POM reformate but not as good as the SMR reformer [29]. The advantage though, is the gained thermally neutral system component, more responsive than a SMR reformer, moderate in cost, size and weight requirements. The drawback is that more extensive control system is needed for ATRs to ensure proper robust operation of the fuel processing system.

2.5 Dry Reforming Of Methane

DRM is a well-defined reaction that is of both scientific and industrial importance mainly due to the desirable consumption of CO_2 as a GHG. The DRM was first studied by Fischer and Tropsch in 1928 over Ni and Co catalysts and since then DRM was continuously investigated by a large number of studies. However, a breakthrough that will industrialize this method has not been achieved yet [30].

DRM is an endothermic reaction that requires operating temperature of 900–1273 °K and pressure close to 1 bar in order to attain high equilibrium conversion of reactants (CH_4 and CO_2) to products (H_2 and CO). These temperature –pressure ranges also minimize the thermodynamic driving forces that lead to high carbon deposition and reduce the catalyst stability [31, 32].

DRM is inevitably accompanied by catalyst deactivation due to carbon deposition. A close relationship is established between the carbon deposition mechanism and the (i) reactant composition, (ii) active metal type and composition, (iii) mesoporous support type, (iv) active metal-support interactions and also to the (v) catalyst preparation methods [33-35]. The DRM main reaction (Eq. 1) is followed by three side reactions (table 2): (i) methane decomposition (Eq. 11), (ii) Boudouard reaction (Eq. 12) and (iii) Revers water gas shift (RWGS) reaction (Eq. 13). The studies of carbon deposition minimization through thermodynamics and reaction mechanisms use the Gibbs free energy methods [36-39] and show that the first two are responsible for the deactivation due to carbon deposition. Methane decomposition (Eq. 11) is thermodynamically favored with low temperature while high temperature favors the Boudouard reaction (Eq. 12).

Table 2: The DRM reactions

Reaction Designation	Reaction	ΔH^0_{298K} kJ·mol^{-1}	ΔG^0	Reaction Priority	Eq.
DRM	$CH_4 + CO_2 \leftrightarrow 2CO + 2H_2$	247	61770- 67.32T	Main Reaction	(1)
Methane Decomposition (Methane Cracking)	$CH_4 \leftrightarrow C + 2H_2$	75	29960- 26,45T	Side Reaction	(11)
Boudouard (CO Disproportionation)	$2CO \leftrightarrow CO_2 + C$	-171	-39810+ 40.87T	Side Reaction	(12)
Revers Water Gas Shift (RWGS)	$CO_2 + H_2 \leftrightarrow CO + H_2O$	41	-8545+ 7.84T	Side Reaction	(13)

Several different kinetic models are used to illustrate the reaction mechanisms and the most widely used models are the (i) Power Law [40] (ii) Eley Rideal (ER I and II) [41] and (iii) Langmuir Hinshelwood–Hougen Watson Model (LHHW or LH) [42]. Various rate models can usually fit certain experimental data, using numerically integrated rate equations, while typically one model is found to have best agreement with the experimental results. This model is usually the one that contains a complete subset of reactions necessary to describe the network of reactions that are known to occur at the experimental reaction conditions.

The most commonly used catalysts for DRM are based on Ni [43], whereas these catalysts undergo severe deactivation processes due to carbon deposition. Noble metals [35, 44] [45-47] have demonstrated much more resistance to carbon deposition than Ni catalysts, but are generally uneconomical and requires their integration as second metal in low percentage over Ni based catalysts.

2.6   Tri Reforming

Tri-Reforming is a synergetic combination of endothermic DRM (Eq. 1) and SMR (Eq. 2) and exothermic oxidation of CH_4 (Eq. 3 and Eq. 4). With this process concept, CO_2, H_2O, and O_2 in the flue gas from fossil-fuel-based power plants can be utilized as co-reactants for tri-reforming of methane for the production of syngas (Figure 6) [48]. Tri-reforming thermodynamics shows that it can be carried out with various feed gas compositions which are not limited to specific gas mixtures.

The tri-reforming concept as an advanced approach to CO_2 conversion uses flue gases for syngas production. Coupling DRM and SRM provides syngas with desired H_2/CO ratios for methanol and F-T synthesis [48].

The combination of dry reforming with steam reforming can accomplish two important missions: producing syngas with desired H_2/CO ratios and mitigating the carbon formation problem that is significant obstacle for DRM. Integrating SMR and POA with DRM could dramatically inhibit carbon formation on reforming catalyst by oxidizing the coke to increase catalyst life and process efficiency.

Song [48] reported that Catalytic tri-reforming of methane was achieved successfully with high CH_4 conversion ($\geq 97\%$) and high CO_2 conversion (around 80%) for producing syngas with desired H_2/CO ratios of 1.5–2.0 over supported Ni catalysts at 1130-1273 °K and 1 bar without carbon formation on the catalyst.
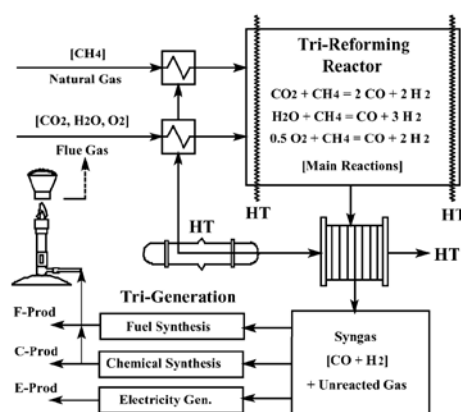

Fig. 6. Process concept for tri-reforming using flue gas from fossil fuel-based power plants. HT represents heat transfer or heat exchange including reactor heat up and waste heat utilization.

2.7 Comparison of Different Reforming Technologies

Reviewing the syngas production methods shows that they are divided into the developed-mature processes such as the SMR and the POM and into the undeveloped methods. Currently all methods involve high costs and are subjected to similar deactivation mechanisms. Basically, SMR requires high heat supply and produces products with a H_2/CO ratio ~ 3:1 that is relatively higher than that for the F-T synthesis. In addition, POM reactor would be more economical to heat than the SMR and the process can be utilized without catalyst. The produced syngas with a H_2/CO ratio of 2:1 is ideal for downstream F-T processes. However, the POM requires costly air separation plant for O_2 supply and special equipment for reacting temperatures as high as 1770°K. Moreover, The ATR reactor in comparison to the SMR is moderate in cost, size and weight requirements. The main drawback is that relatively extensive control system is needed for ATRs to ensure proper robust operation of the fuel processing system. The tri-reforming Integrates SMR, POA and DRM which can dramatically inhibit catalyst deactivation by

18

oxidizing the coke to increase catalyst life and process efficiency and can utilize flue gases from fossil-fuel-based power plants as co-reactants for the production of syngas.

In comparison to the SMR, POA ATR and tri reforming, DRM has its unique advantage because of its novelty in the utilization of CO_2 which offsets the increasing GHG emissions. However, this reforming method is still challenged with various issues and further development is requisite in the near future.

3   CATALYSTS DEVELOPMENT FOR DRY METHANE REFORMING

Heterogeneous catalysts for the DRM (are defined as a catalyst in a solid phase different from the gas phase of reactants. The heterogeneous catalysts accelerate the reforming reactions without being consumed but being subjected to properties changing due to deactivation mechanisms. The heterogeneous catalyst design begins with the proper combination of the active metal and support to the designed reforming conditions and also includes various range of perpetration methods to control the chemical reactions and the crystallographic structures of the active metal and the support. In addition, promoters are non-active additives that are used to improve the metallic dispersion over the support, minimizing carbon deposition and active metal sintering.

The criteria for a good heterogeneous catalyst considers activity, selectivity, thermal and mechanical properties, stability, morphology, ease of regeneration, low toxicity and low cost [49-51]. These criteria is achieved and characterized by:

a) The relative volumes of the active metals, chemical promoters, selective blocking additives, and the supports [52].
b) Keeping the active metal nanoscopic scale of 1-10 nm, support particles of 20-50 nm, and porous support body macroscopic scale of 1-2 mm [51].
c) Gaining high surface area, proper mesoporous volume and high active metal distribution [51].

3.1   Active Metal Species for the DRM

Increasing attention from both academia and industry is paid to the DRM process in order to produce syngas of low H_2/CO ratios as feedstock for the GTL technologies [53]. Basically, the active metal catalysts belong to Group VIII and are divided to two groups: earth-abundant transition metals and noble metals. The majority of catalysts nowadays are based on Ni due to its high activity and its market price. Catalyst deactivation mechanisms lead researchers to combine other metals such as Co or noble metals to create bimetallic alloy for property improvement. The noble metals, Rh, Ru, Ir, Pt and Pd have promising catalytic performance and low sensitivies to carbon deposition. However, their unavailability and high cost limit their utilization as a single metal catalyst in large-scale processes.

3.1.1   Ni Based Catalyst

The Ni metal is catalytically active for the dry reforming reaction, but excess carbon deposition on the surface causes the catalyst deactivation [54-56] . The deposited carbon is originated via methane decomposition (Eq. 11) [38, 39, 57, 58] and/or CO disproportionation (Eq. 12) with dependence on the thermodynamic variables and active metal species [59]. Researchers are

focusing on the improvement of the Ni based catalyst by addition of promoters [33, 60-65], using different supports [39, 66-81] and advanced reactors configurations [15].

Although noble metals were proved to be less sensitive for carbon depositions [16, 39, 68, 75, 77, 82-86] it is required to develop supported Ni-based catalyst due to its relatively low cost and high availability.

Ni catalyst structure is closely related to the carbon deposition for DRM and studies that were published recently were devoted to clarify the relationship between the carbon formation of supported Ni catalysts and the morphology of metal particles [59, 81, 87, 88]. According to these studies, the carbon forming tendency of supported Ni catalysts may have a close relationship with the metal particle size. Supported Ni catalysts that were prepared by conventional impregnation method [89, 90] could not offer a clear explanation about the effect of metal particle size on coke formation because the morphological control of metal particles was limited. On the other hand, the metal particle size could be properly controlled by adjusting Ni loading in the preparation step of sol–gel process and subsequent supercritical drying and thermal treatment [89].

In order to find the relation of the particles metal morphology and the catalysts deactivation by coke formation, Kim *et al*. [89] prepared Ni/Al_2O_3 catalysts with various Ni loadings by aerogel method. This study demonstrated that the high-surface area Ni/Al_2O_3 catalysts with high mesoporosity are suitable catalysts for DRM. Good textural properties and stability during the thermal treatment up to 973 °K led to the formation of small Ni particles dispersed uniformly on the Al_2O_3 support. The control of metal particle size could be achieved by varying the Ni loading. Catalyst deactivation caused by both carbon formation and sintering of Ni particles. Although aerogel catalysts showed good catalytic performances with respect to activity and stability, it was difficult to avoid carbon formation during the DRM reaction. The large Ni particles formed in the catalyst preparation and/or the reaction steps are susceptible to the growth of whisker carbon. It was concluded that a minimum diameter of about 7 nm is required for the Ni particles to generate deposited carbon and metal sintering.

In order to prove the assumption that better dispersion and small particle size reduce catalyst deactivation, a SiO_2 support was prepared [91] by flame spray pyrolysis (FSP) for Ni catalysts. The variations in SiO_2 properties altered the (5 wt %) Ni deposit characteristics which in turn impacted on the DRM reaction. It was proved that as the SiO_2 surface area increased, the Ni dispersion increased and the catalyst performance improved.

Similarly, using a mesoporous SiO_2 support, a series of Ni samples (Ni/SiO_2) [92] were tested with different Ni content (3.1%–13.2%). Results showed that the highly dispersed 6.7% Ni/SiO_2 catalysts, compared with other contents of Ni/SiO_2 catalysts, exhibited excellent catalytic activity and long-term stability. The metallic Ni particle size was significantly affected by the metal anchoring between metallic Ni particles and unreduced Ni ions in the SiO_2 matrix. The

strong anchoring effect was suggested to account for the retention of small Ni particle size and the improved catalytic performance.

In order to relate the contribution of the nickel-support interaction , Alak *et al.* [93] showed that the reduction of the Ni aluminate would result in the formation of small Ni particles, which are resistant to sintering and carbon formation. A Ni/Al_2O_3 catalyst was prepared at 733 $^\circ$ K and showed relatively low carbon deposition but also poor activity and stability due to the formation of the spinel structure of Ni aluminate. Observation of the calcination temperature effect indicated that the Ni/Al_2O_3 catalyst prepared at 1123°K presented good activity and stability for 70 h although the amount of carbon deposition was higher than on the 733°K calcined Ni/Al_2O_3 catalyst. It was concluded that the deactivations originated from two different type of carbon formed on the catalysts during reforming: amorphous carbon covered all the active metal, but the filament carbon that was grown did not cover the metal surface.

3.1.2 Noble Metal Based Catalysts

Thermodynamic analysis shows that DRM requires reaction temperatures as high as 1173 °K to attain high syngas yields. Although Ni is the preferred metal as catalyst for the DRM [47, 82, 94-100], industry constraints lead science to continuously look for ways of mitigating carbon deposition [16 , 39] and irreversible undesirable reactions with the support (*e.g.,* forming inactive spinels) [78].

Noble metals (or precious metals) were found promising for the inhibition of catalyst deactivation thanks to their high selective and stable reactivity, higher resistance in high temperature applications [101] and their significant reaction energy reduction. However, their high market price still challenges their employment in industrial scales and motivate researchers to examine their implementation as second metal in low percentage in bimetallic catalyst based on Ni or Co. The noble metal characteristic that provides their best functionality in reforming processes are [101, 102]:

A. The ability to be dispersed into nanoscale particles better than most of other transition metals which can easily adsorb H_2/O_2.
B. The electrons presented in the filled d-subshell (being more exposed) promote the dissociative adsorption of H_2/O_2.
C. The relatively easiness of noble bimetallic catalyst preparation by the impregnation method.

3.1.3 Ruthenium and Rhodium

In order to explore the noble metal effectivity, the catalytic activity and stability of Rh, Ru, Pd, Ir and Pt were investigated both as monometallic catalyst in comparison to a non-noble metal monometallic catalysts and also as a bimetallic combination of noble and non-noble metals.

The Ru and Rh show best resistant among the noble metals, [103, 104] toward catalyst deactivation by carbon deposition. The activities of the noble metals have been systematically compared in terms of turnover numbers, however, analysis of results presented by different groups, reveals inconsistencies when comparing the relative catalytic activity of these metals [80].

In similarity to abundant earth metals, it was shown that the noble metal exhibit different activity with dependence on the support type due to chemical reactions between the two [105-107]. This modification to the activity of the metallic phase has been interpreted in terms of the structure sensitivity of the reaction and also from the perspective of changes in the reaction mechanism induced by participation of the support in the activation of either CH_4 or CO_2 [107]. Considering the fact that the support participates in the activation it is anticipated that the noble metal-support interface plays a significant role in the DRM reactions.

Bradford [94] showed that the activity and selectivity of Ru catalysts highly depend on the oxidation state of the metal, which can change according to the reaction conditions and the support. Bradford [94] also proved that the support can have a significant influence on the type of carbonaceous species formed during reaction. Ferreira et al [108] checked the catalytic performance over Ru catalysts supported on γ-Al_2O_3 and found that the Ru sites are able to activate CO_2, but CO_2 is more efficiently activated on the γ-Al_2O_3 support. The explanation for this result is that CO_2 readily adsorbs to the support basic sites and generally has a larger binding energy on metal oxides compared to metal surfaces. Overall, the interface between the Ru particle and the support is believed to be the active sites for CO_2 adsorption, and the dissociation of the CO_2 molecule may proceed by a hydrogen-spillover-like mechanism [76].

Nagaoka et al. [109] added to the above and checked the support effects over the catalytic behavior of Ru (2.0 wt.%) catalysts, under low and high pressure and shown that the activity order under pressure of 1 bar was consistent with the basicity of the support in the order of Ru/MgO>Ru/Al_2O_3>Ru/TiO_2>Ru/SiO_2, indicating that the CO_2 adsorption (as carbonate type species) on the supports determines the catalytic activity. When reaction pressure was elevated to 20 bar, a difference of the activity was observed due to a different kinetic mechanism, and the order of activity was Ru/SiO_2>Ru/Al_2O_3>Ru/MgO>Ru/TiO_2. The support basicity affected the Ru activity at 0.1 MPa while other mechanism influenced the reactivity at 20 bar. When examining the Ru particle size as a result of sintering, Nagaoka et al. [109] showed that the order of Ru particle size was Ru/TiO_2>Ru/SiO_2>Ru/MgO>Ru/Al_2O_3, concluding that the Al_2O_3 has best effect of inhibiting the Ru metal sintering.

Following the Ru, the Rh also show highest activity and resistance to carbon deposition [105, 106]. However, Ferreira [110] showed that in similarity to Ru, the stability and durability of the Rh active sites are effected by the catalysts support and acts in different reaction mechanisms. Over SiO_2 support, which is considered to be the most inert [110], the whole reforming process occurred on the Rh phase and led to relatively more rapid ageing of the catalyst. The rapid ageing was related to a large residence time of surface carbon intermediates favoring

polymerization and graphitization. Less inert supports (*e.g* Al_2O_3) act as a collector of CH*x* species which reduces the residence time of carbon species on the Rh phase and therefore leads to more stable catalysts.

3.1.4   Comparison of Ru and Rh with Other Active Metals

Numerous studies in the last decades compared the activities of the noble metals in order to determine which noble metal performs best in activity and resistance to carbon deposition. Hou *et al.* [111] compared the stability and reactivity of Rh (5 wt%), Ru (5 wt%) and Ni (10 wt%) as supported metals. The noble metals showed higher coke resistance ability, while their activity was relatively low in comparison to Ni. In comparison to the Ru, the Rh in this study presented higher dispersion on the mesoporous Al_2O_3 and exhibited higher coke resistance and higher reforming activity. In contrary to Hou *et al.* [111], additional studies [112-114] showed that Ru and Rh presented higher activity in comparison with Ni and also higher activity than Pd and Pt. It is concluded that the activity dependency on supports and thermodynamic conditions is still not fully determined.

Hou *et al*. [115] investigated the effect of different noble metals (Rh, Ru, Pt, Pd and Ir) supported on Al_2O_3 and concluded in agreement with Matsui [116] that noble metal (5 wt%) supported catalysts lead to high coking resistance and stability in the order of Rh >Ru >Ir >Pd >Pt. In similarity to previous study by Hou *et al* [111], the Rh showed best performance, followed by Ru. The amount of deposited carbon over these Al_2O_3 supported catalysts was highest for Pd with 4.9 (mgcat/gcath) while rest of them showed almost no carbon deposition.

Usman [117] proved that the relatively low stability of Pt and Pd supported catalysts is related to the sintering of the metal particles at higher reaction temperatures and also on kinetic mechanism, effected by the support. Noble metals that were tested over Mg−Al double layered hydroxides support ($MgAlO_x$) [117, 118] at 1073 °K for 50 h, showing coke deposition order of Pd > Pt >Ir >Rh >Ru. It was concluded that for $MgAlO_x$ support under the stated condition the highest catalytic stability and lower carbon deposition was achieved by the Ru.

3.1.5   Bimetallic Catalysts

Although Ni, Ru and Rh catalysts have gained much attention as active metals for the DRM process, attempts are continually made to improve the catalyst activity, process stability and process cost. Carbon deposition and metal sintering are still great challenges that hold the DRM from being industrially used. In addition to the modification of the supports to improve the stability of Ni catalyst for DRM, different active metals such as Co, Fe or noble metals Rh, Ru, Pt, Ir and Pd [24, 25, 67, 80] are added in small amounts to the base active metal, creating bimetallic catalysts for of carbon depositions inhibition improvements.

Ni-Co Based Catalyst

The cobalt was found as appropriate candidate for bimetallic catalyst due to its higher melting and vaporizing points in comparison to the Ni and its lower price in comparison to the noble metals.

Al-Fatesh [119] show that the interaction of bimetallic Ni-Co catalysts provided higher activity and less carbon formation. The addition of Co leads to a strong adsorption capacity [120] of CO_2 which favors the elimination of carbon. Similar researches results [77, 121, 122] also demonstrate that the catalyst activity and stability can be improved through formation of a homogeneous bimetallic alloy, which performs better than the corresponding monometallic catalysts.

Zhang *et al*. [123] showed that the change of the metal dispersion and metal particle size on Al_2O_3-MgO support facilitated improved activity and coke suppression of Ni–Co bimetallic catalysts. Catalyst samples were characterized with Ni and Co loadings ranging between 1.83 and 14.5 wt. %, and 2.76 and 12.9 wt. % respectively. Using the TEM, XRD, H_2-TPR, TG/DTG-TPO, N_2-physisorption and CO-chemisorption they indicated that catalyst with low Ni-Co content (1.83–3.61 wt.% for Ni and 2.76–4.53 wt.% for Co) has larger surface area, smaller metal particles and better metal dispersion and therefore gives rise to better catalytic performance. The absence of large metal particles (>10 nm) was essential to the complete suppression of the carbon formation during reaction.

A bimetallic Co–Ni/TiO_2 catalyst showed highly stable activities [99]. The small Ni substitution of cobalt (10 mol%) dramatically improved the catalytic activity and stability. The monometallic cobalt catalyst Co/TiO_2 was deactivated rapidly due to the oxidation of metal during the DRM reaction. The bimetallic Co–Ni catalysts improved its resistance to oxidation, forming titanate that leads reactivity toward methane decomposition (Eq. 11) and providing a more reductive atmosphere over the catalyst (e.g., H_2 as a product). With the excess content of Ni (>80 mol%), the catalyst showed higher activity for the methane decomposition (Eq. 11) and for the reforming, but also caused more carbon formation. It was concluded that with appropriate adjustment of the ratio of Co-Ni loading, the catalyst provides an optimum balance between the DRM reactions and catalyst deactivation. The using of MgO−ZrO_2 support [124] for Ni−Co bimetallic catalysts lead to a CH_4 conversion of 80% for Ni−Co/MgO−ZrO_2 in comparison to the monometallic Ni 70% and Co 71% .

These results show the advantage of utilizing bimetallic catalyst and are attributed to the better metals dispersion, smaller particle size and to the synergic effect between Ni and Co.

Ni-Fe Based Catalyst

Iron is not commercially used as catalyst for reforming reactions due to its low reactivity, however, researchers proved that together with perovskite type catalysts, the Fe can contribute

to the Ni stability [25] due to its high melting and vaporizing points, in similarity to the cobalt. Lu *et al*. [125] explained the motivation to investigate the Fe effect when compared the thermodynamic and kinetic mechanism of carbon deposition over Fe, Co, and Ni monometallic catalyst in CO_2/CH_4 mixtures and that the carbon deposition order was Fe << Co << Ni.

Nam and Lima [126][127] showed that catalyst precipitation and calcination with small amounts of Fe can improve the stability of the alloyed catalyst. $LaNi_{(1-x)}Fe_xO_3$ (x=0, 0.2, 0.4 and 0.7) perovskite-type catalysts were modified by the partial substitution of Ni by Fe, aiming to increase the stability and resistance to carbon deposition. The catalyst was tested and exhibited similar activity and selectivity to the noble metals but was deactivated quickly due to carbon deposition. The results showed that certain additives and proper combination of precipitation and calcination methods could resulted in oxides with the desired structure and with improved properties [126][127][25, 113, 128, 129].

From a practical viewpoint the most active abundant earth catalyst is Ni, in comparison to bimetallic addition of Co, Ce and Fe [83], the order of the activity is : Ni, Ni–Co, Ni–Ce > >> Ni–Fe. However, high carbon deposition on the Ni catalyst reduces the catalyst stability and is proposed to be mitigated by the utilizing of bimetallic solution.

Combined Ni or Co and Noble Metals

The utilization of bimetal catalysts based on Ni or Co with noble metals as an additive is also proposed to account for DRM catalyst improvement [112, 114, 118, 130-132].

Ghelamallah [112, 115] investigated the modification effect of Rh to a Ni catalyst supported over mesoporous Al_2O_3 and showed that the Ni catalyst without Rh addition exhibited higher coke formation rates (17.2 mgcoke/mgcath) and lower methane (62.0%) and carbon dioxide (68.0%) conversions. This higher stability and activity was attributed to the synergic effect of Rh and Ni, which leads to the formation of Rh–Ni cluster over Al_2O_3 support. Similar results were reported for Pt-Ni bimetallic catalyst ($0.4Pt-Ni/\gamma-Al_2O_3$) [132], which exhibited highest activity of 69% CH_4 conversion compared to the monometallic $4Ni/\gamma-Al_2O_3$ and $0.4Pt/\gamma-Al_2O_3$ catalysts that presented CH_4 conversion of 60% and 65% respectively.

Tomishige [133] showed that the addition of small amounts of Pt, Pd and Rh to $Ni_{0.03}Mg_{0.97}O$ catalysts promoted a significant increase in activity. The improved performance was attributed to the segregation and exposure of noble metal on the surface of the catalyst. Similar results were achieved when checked the Ni–Ru and Ni–Pd bimetallic catalysts supported on SiO_2 [132]. It was shown that the Ni–Ru had notably higher activity than the Ni–Pd and the Ni monometallic catalyst. The higher activity was attributed to an enrichment of Ni–Ru clusters.

Tsubaki *et al*. [134] prepared bimetallic Co catalysts with the addition of different noble metals. The Pt and Pd slightly increased the Co reducibility but successfully formed well-dispersed alloy with Co. The well dispersed alloy enhanced the turnover rate and also showed high

methane selectivity which was attributed to the small metallic Co particles and H_2 spillover effect (providing electrons to the Co). However, same experiment showed that Ru improved Co reducibility greatly but had only a slight effect on Co dispersion due to the formation of two distinct phase's structure. This structure was formed during the reduction step of the catalyst preparation. This kind of structure variance determined the different reaction behavior of Pt-Co, Pd-Co, and Ru-Co catalysts, while most of the Pd and Pt was embedded in the bulk phase of Co or CoO_x, ineffective to the reduction of supported cobalt oxides. The catalytic activity of the Co based bimetallic noble catalysts was concluded to follow the order of Ru-Co > Pt-Co > Pd-Co > Co [134].

It has been demonstrated that the activity and stability of Ni and/or Co catalyst can be significantly improved with the addition of noble metals [79, 112, 115, 135] and Ru provides best results in comparison to the other noble metals. However, the real mechanism for this increase in activity is not yet fully understood and has to be further studied in order to find the best combinations that will lead to the most efficient DRM process concerning the catalyst stability and activity and catalyst costs.

The role of active metals in the enhancement of catalytic activity is listed in Table 3. It can be seen that the highest conversions and in ratio close to unity are obtained with the utilization Ni/Al_2O_3 catalyst.

Table 3: The role of active metals in the enhancement of catalytic activity.

Metal	Support	Metal Weight %	Preparation Method	Temp K	Time In Reactor Hours	Reactor Type	CH_4 Conversion %	CO_2 Conversion %	Ref.
Ni	Al_2O_3	10	Impregnation	800	30	FBR	63.0	69.0	[136]
			Sol–gel		48	FIBR	94.0	93.0	
Co	γ-Al_2O_3	20	Sol–gel	700	20	FBR	32.0	39.0	[137]
					20	FIBR	66.0	71.0	
Ni	CeO_2	10	IWIMP	550	7	FBR	58.0	69.0	[138]
Ni	ZrO_2	5	IWIMP	750	10	FBR	65.0	-	[139]
Pt	ZrO_2	1	Impregnation	700	4	FBR	79.0	86.0	[140]
Rh	CeO_2	0.5	Impregnation	800	50	FBR	50.7	63.2	[141]
	ZrO_2						65.9	74.2	
Pt	Al_2O_3	1	Impregnation	800	97	FBR	46.0	62.0	[142]
	ZrO_2						83.0	94.0	
Ru	Al_2O_3	3	Impregnation	750	20	FBR	46.0	48.0	[101]
	CeO_2	2					52.0	60.0	
Co	MgO	12	Impregnation	900	0.5	FBR	91.9	93.9	[143]
Ni	MgO−SiO_2	5	Impregnation	700	--	FBR	58.3	-	[144]
Pt−Ni		0.01–5					80.7	-	

Catalyst	Support	Loading	Method	Temp	Time	Reactor	Conv.	Yield	Ref
Ni	SiO_2	5					55.0	-	
Ni	CeZr	5	Impregnation	750	70	FBR	41.0	-	[145]
Ni	$Ce_{0.8}Zr_{0.2}O_2$	15	CP	800	42	FBR	78.0	77.0	[146]
Ni−MgO		15−10			200		95.0	96.0	
Ru	Al_2O_3	5			--		91.0	90.0	
	CeO_2	5	Impregnation	750	--	FBR	90.0	96.0	[147]
Ru−Ce	Al_2O_3	5 and 3			--		97.0	97.0	
Ni	MCM-41	1.2	DHT	750	30	FBR	7.0	-	[148]
Ni-Rh	MCM-41	0.19	DHT	600	4	FBR	20	38.0	[149]
Ni	SBA-15	12.5	Impregnation	800	720	FBR	43	70	[150]
Ni-Mo	SBA-15	5-25	IWIMP	800	120	FBMR	84.0	96.0	[151]
Ni	SiO_2	4.5	IWIMP	750	11	FBMR	47.0	60.0	[152]
Ni-Ce	SiO_2	10-5	IWIMP	800	30	FBR	81.4	87.5	[153]
Rh	SiO_2	0.5	Impregnation	800	50	FBR	71.9	77.2	[141]
$La_{0.8}Sr_{0.2}Ni_{0.8}Cu_{0.2}O_3$	PTO	4.9	Sol–gel	800	24	MR	75	60	[154]

CP: co-precipitation; SG: Sol−gel; IWIMP: incipient wetness impregnation; DHT: direct hydrothermal synthesis; FBR: fixed bed reactor; FIBR: fluidized bed reactor; MR: micro reactor; FBMR: fixed bed quartz micro-reactor; PTO: perovskite-type oxides.

3.1.6 Summary of Active Metal Species for the DRM

It can be concluded that Ni is widely recognized as the best base metal for bimetallic alloys of both earth abundance metals and noble metals. The bimetallic catalysts show significantly higher catalytic activities and better stability compared to monometallic Ni catalysts. However, the catalytic activity of the bimetallic catalysts increased gradually with noble metal loading while after passing through a maximum it decreased with superfluous noble metal addition. Although deactivation of catalyst leads to an integration of noble metals in the catalysts, their high market prices and low abundance are still significant factors that enforce their utilization as bimetallic additives in small amounts rather than a monometallic catalyst.

3.2 Catalyst Support

3.2.1 Support Effects for DRM

Catalysts are often simplified by considering them as being composed of two independent and isolated phases, *i.e.* the metal as the catalytically active component, and the support which acts as the mesoporous substrate where the metal is dispersed, and is normally considered as being inert itself for the reaction. However, this is clearly an over-simplification, given that supported and unsupported metals behave differently for CH_4 activation in DRM [107]. The mobility and migration of adsorbed species from the metal to the support and *vice versa* can take place to a significant extent for supported catalysts, under conditions (*i.e.* high temperatures) where the methane decomposition (Eq. 11) and the CH_4+CO_2 reaction proceed. These processes sometimes lead only to the removal of reactants and the formation of spectator species but in other cases they may be involved in the reaction and give rise to changes in the pathway when compared with isolated metallic surfaces.

A significant factor effecting carbon deposition is the catalyst surface basicity [155]. In particular, it has been demonstrated that carbon formation can be diminished or even suppressed when the active metal is supported on a metal oxide carrier with Lewis basicity [155]. Proper selection of the support can significantly modify the catalytic properties of a given metal on DRM conditions and change the tendency towards sintering prevention and resistance to carbon deposition.

Ni based catalysts were proved to be the most attractive for DRM processes [138] while being subjected to deactivation which lead to the development of heterogeneous catalysts with improved activity and selectivity. The catalyst support, which may be inert or participate in the catalytic reactions [125], has major effect of the catalytic performance. Great efforts are made to maximize the catalyst surface area by better dispersion of active metal over the mesoporous support. Mesoporous supports with a hierarchical structure from a family of silicate and alumosilicate solids, have been two of the most often investigated catalysts for DRM in the last decades [156].

3.2.2 Catalyst Supports for DRM

Among the various transition Al_2O_3, the γ-Al_2O_3 is one of the most important catalyst support in petroleum industries catalytic processes [157-159]. The γ-Al_2O_3 textural properties, such as surface area (95-375 m^2/g) [160], pore volume and pore-size distribution are mainly owed to surface chemical basic composition, local microstructure and phase composition [78, 161-163]. The microstructure and thermal and hydrothermal stability of the material is strongly depend on the preparation methods [164]. The acid/base properties of γ-Al_2O_3 with tendency to basic greatly promote the catalyst activity since CO_2 is as an acid gas in which adsorption and dissociation are improved with the basicity [165].

31

A comparison between MgO, CeO$_2$, ZrO$_2$ and γ-Al$_2$O$_3$ [166-168] showed that although Ni/CeO$_2$ had the best dispersion among the supported nanocatalysts, Ni/Al$_2$O$_3$ showed the highest H$_2$ and CO yield due to its high surface area, homogenous distributions and the high dispersion of Ni. A low cost clinoptilolite [169] support was compared to CeO$_2$ and Al$_2$O$_3$ [170] for the purpose of cost reduction. The Ni/clinoptilolite presented relatively good activity. However, its H$_2$ and CO yields as well as H$_2$/CO molar ratio were lower than that of Ni/Al$_2$O$_3$. This finding reduced the interest of commercializing this support material.

Al-Fatesh [171] revealed that while Ni/γ-Al$_2$O$_3$ provide better catalytic activity than Ni/MgO, it was more sensitive to the amount of Ni that reduced its activation when overloaded. Both supports demonstrated almost identical coking rates on the surface of the catalyst. However, due to the poor mechanical strength of MgO in comparison to Al$_2$O$_3$, it attracted relatively little interest for industrial use researches [172].

Besides the γ-Al$_2$O$_3$ support, SiO$_2$ is of the most often investigated catalyst for DRM since 1980 [173]. Three SiO$_2$-based mesoporous materials, MCM-41, SBA-15 and KIT-6 which have different pore diameter and surface area are most interesting as support, having melting point is 2318 °C [150, 174, 175]. The SiO$_2$ support is also considered as the most inert support among Al$_2$O$_3$, MgO and TiO$_2$. This fact is favorable when a catalytic reaction mechanism without support interference is required [176].

Amin and Liu *et al.* [79, 148, 156] compared SBA-15, KIT-6, MCM-41 and γ-Al$_2$O$_3$ using Ni as the active metal. Among all the supported catalysts the Ni/SBA-15 exhibited the best catalytic performance in terms of catalytic conversion and long-term stability. The excellent performance of the SBA-15 based catalysts, correlated strongly with its unique mesoporous structures that inhibit carbon formation and minimize the active Ni sintering [174].

Ferreira *et al.* [108, 110] showed (Table 4) the active role of the support when compared Ru/SiO$_2$ to Ru/Al$_2$O$_3$ at 823 °K. It was shown that the Ru amount is lower onto the Al$_2$O$_3$ support and that the dispersion, conversion and conversion rates are higher. The reason for the Al$_2$O$_3$ superiority is the support effect over the kinetic-mechanics path of the reaction. The Ru over the Al$_2$O$_3$ support provided a better alternate route for CO$_2$ activation by producing intermediates on its surface. The subsequently decomposed intermediates released CO and gained reduction of coke formation. However these results doesn't controvert with Amin and Liu's results since long term stability wasn't checked by Ferreira.

Table 4: Selected catalytic properties of supported Ru catalysts over SiO$_2$ and Al$_2$O$_3$ at 823 °K

	Ru/SiO$_2$	Ru/Al$_2$O$_3$
Ru content (%)	0.72	0.64
Initial dispersion (%)	13	51
CH$_4$ conversion (%) (t=10 min)	12	14
r$_{CH_4}$ (μmol g^{-1} s^{-1}) (t=10 min)	29.9	34.1

Similarly Joyner [176] showed that higher temperatures is favored with the SiO_2 but not with the Al_2O_3 support for CH_4 conversions, providing 52% and 57% conversions for the Ru/Al_2O_3 and Ru/SiO_2 at 1023 °K respectively. The loss of activity resulted from a slow and continuous sintering of the metallic phase over the Al_2O_3 support.

The TiO_2 support is often preferred over SiO_2 due to its basicity characteristic. Nagaoka [109] revealed that the strong resistance to coke deposition for Ru/TiO_2 may be attributed to the characteristics of the metal catalysts supported on TiO_2, called strong metal support interaction (SMSI) [177]. It has been shown that TiO_2 supported metal catalysts suppress coke deposition during the DRM (Table 5), most probably due to the decoration of metal particle surfaces by TiO_x species (SMSI). The TiO_x species destroy large ensemble of metal atoms that serve as active sites for carbon deposition through the methane decomposition (Eq. 11) and CO disproportionation (Eq. 12) reactions [105].

Table 5. The amount of coke deposition on supported Ru catalysts after reaction of 25 h over 1 and 20 bar.

Catalyst	Coke deposition (wt. %)	
	1 bar	20 bar
Ru/SiO$_2$	nd (<0.7)	16.4
Ru/Al$_2$O$_3$	nd	19.5
Ru/MgO	nd	1.2
Ru/TiO$_2$	nd	nd

nd: no detected deposition

Table 6 demonstrates that the Ni supported catalysts shows the best activity among the earth abundance active metals and gets the highest literature cover followed by the noble metal Rh while the Al_2O_3 support followed by the TiO_2 shows the best reforming performance.

Table 6: Catalytic performance over different supports.

Activity Order Per Active Metal	Reforming temp °K	Metal loading wt.%	Ref.
Ni			
$Al_2O_3 > ZrO_2 > TiO_2 > CeO_2 > MgO$	823	12	[178]
γ-$Al_2O_3 > TiO_2 > ZrO_2$-CP $> ZrO_2$-AS $> SiO_2$	1073	5	[179]
$La_2O_3 \sim SiO_2 > \alpha$-$Al_2O_3 \sim MgO > CeO_2 > TiO_2$	973	5	[180]
Mo₂C (Molybdenum Carbide)			
$Al_2O_3 > SiO_2 > ZrO_2 > TiO_2$	1220	3.8	[159]
Rh			
$Al_2O_3 > TiO_2 > SiO_2$	773	0.55	[181]
$Al_2O_3 > TiO_2 > SiO_2$	773	0.5	[159]
$TiO_2 > La_2O_3 = CeO_2 > ZrO_2 = MgO = SiO_2 = MCM$-41 $> \gamma$-Al_2O_3	973	0.5	[182]
Yttria-Stabilized Zirconia (YSZ) $> Al_2O_3 > TiO_2 > SiO_2 > La_2O_3 > MgO$	873	0.5	[67]
Ru			
YSZ $\gg SiO_2 > TiO_2 > ZrO_2 > \gamma$-$Al_2O_3$	700	0.51-0.64	[183]
Pt			
$TiO_2 > Al_2O_3 > SiO2$	723	4	[184]

Pt-Sn			
$Al_2O_3 > TiO_2 > SiO2$	723	4	[184]
Pd			
$TiO_2 > Al_2O_3 > SiO_2 > MgO$	823	5	[180]
Ir			
$TiO_2 > ZrO_2 > Y_2O_3 > La_2O_3 > MgO > Al_2O_3 > SiO_2$	823	5	[185]

Table 6 shows that the catalytic performance depends strongly on metal–support interactions. This dependence was found to be affected by the nature of the support and the decreasing order of activity correlates directly with the support acidity. Moreover, the catalytic performance is stimulated by the support which effects the active metal dispersion and metal particle sizes.

At least three factors which are directly related to the active metal-support interactions account on catalyst deactivation, *i.e.*, carbon deposition, metal sintering and active metal surface poisoning by species originated from the support. The impact of each of these factors was found to be inherently determined by the support.

In particular, Al_2O_3 and TiO_2 with the high basicity provide the most stable turnover rates. The yttria-stabilized zirconia (YSZ) also promotes high performance but is currently experimentally evidenced for noble metal only. Over the Rh/YSZ catalyst it is found that there exists a lattice oxygen species of the carrier which intensively interacts with CO_2. A spillover of these lattice oxygen species onto the Rh surface contributes to the formation of CO and H_2O [186].The different turnover rates is also correlated with the stabilized species of Rh atom. It is then concluded that the supports can influence the electronic state of Rh atoms, and that Rh metal serves as prominent active species in the reforming reactions [182] .

3.2.3 Summary of Catalytic Supports

It can be concluded that the catalyst support plays an important role and its contribution to the catalysis activity and coke deposition prevention on DRM process is considerable. It was shown that a significant factor effecting carbon deposition is the catalyst surface basicity and that carbon formation can be suppressed or even diminished when the active metal is supported on a metal oxide support with Lewis basicity. With regards to stability, the majority of the studies show that the reaction between the active metal and the support contributes to the catalyst stability in the order of $Al_2O_3 < TiO_2 < SiO_2 < MgO$. However, the contribution to turnover frequencies was found to be higher onto the lower basicity supports in the order of $TiO_2 > Al_2O_3$.

3.3 Promoters

The catalyst promoters [187] are non-active substances that are proposed to improve the catalytic performance through surface structural effects. Promoters enhance the active metal dispersion over the support [188], benefitting from the existence of strong metal–support interaction effect which change the basicity of the catalysts towards more basic state.

The metal-promoter interaction play two key roles: (i) enhancing metallic dispersion to block step sites on metal surface that is associated with carbon nucleation and growth. The promoter keeps the metallic particle size small over reducing and reforming, and (ii) promoting the gasification of the formed coke. Some promoters, like Ag, alter the type of the formed coke over the metal surface from recalcitrant whisker/encapsulating carbon to gasifiable amorphous carbonaceous species [189].

Al-Fatish [33] tested the effects of promoters on catalyst activity and stability without the effect of the metal and/or support by "blank experiment". This experiment was done without catalysts or support but onto quartz wool and found that the promoter didn't affect the catalytic activity. However, this result cannot be valid for the DRM process due to the fact that the effect of promoter is strongly related to the catalyst, support and the interaction between them.

3.3.1 Ca, Ce, Zr and Sr Promoters

Al-Fatesh [33] investigated the impact of Ce and Zr promoters on $Ni/\gamma\text{-}Al_2O_3$ catalyst at 1 bar and temperature range of 773-1073 °K. The results for catalyst stability and activity showed that the Zr promoter with Ni provided the best catalyst activity for CH_4 and CO_2 conversions. Table 7 presents the results of initial and final activities of the catalyst in terms of CH_4 and CO_2 conversions, and average synthesis gas H_2/CO ratios [190].

Table 7. Comparison of DRM performance at 973°K for non-promoted Ni and Ni promoted with Ce and Zr.

| Promoter | Add (wt%) | Conversion | | | | Average H_2/CO |
| | | Initial | | After 9 h | | |
		CH_4 (%)	CO_2 (%)	CH_4 (%)	CO_2 (%)	
No	0.0	76.7	80.2	72.6	75.9	0.98
Ce	0.05	77.4	80.5	72.3	75.4	0.98
	0.15	78.1	77.2	71.7	73.3	0.97
	0.3	75.2	77.6	68.7	73.6	0.97
	0.45	78.1	81.0	69.1	73.8	0.99
Zr	0.05	81.5	79.7	76.5	74.4	1.06
	0.15	82.3	80.0	77.7	75.9	1.04
	0.3	80.8	78.5	73.6	74.1	1.02

The catalytic activity and stability improvement of Zr promoter is attributed to its ability to enhance CO_2 dissociation by providing oxygen intermediates that facilitate the removal of the formed carbon. This gasified carbon is produced in the methane decomposition (Eq. 11) and the Boudouard side reactions (Eq. 12) over the active metal. Al Fatesh [190] also checked the influence of combined Ca, Ce, and Zr promoters on catalyst stability, coke deposition, and H_2/CO ratio. It was shown that 3% Ni/γ- Al_2O_3 promoted with 0.15% Ce and 0.05% Ca exhibited the best performance and resulted in less coke formation.

The addition of Ce promoter into Co based catalyst [191] leads to enhanced catalytic activity. The Ce promoter enhanced carbon gasification by providing additional surface oxygen storage/transfer capacity through redox cycle [192]. The Ce promoted Co based catalyst showed more stability than Ni–Ce/ZrO_2 and as well as non-promoted Co catalyst.

Valderrama *et al.* [194] and Yung *et al.* [195] examined the Ca and Sr promoter effect on a perovskite crystal structure (ABO_3). The $La_{0.9}M_{0.1}Ni_{0.5}Fe_{0.5}O_3$ (M = Sr, Ca) catalyst performance showed that the promoter substitution in the crystal lattice presented higher basicity, providing high oxygen vacancy and activation of the C-H bond and dramatically reduced metal sintering. A similar study used Fe due to its proved contribution on perovskite crystal structure to carbon resistance. However, no such promoters showed contribution to activity increase [25, 154].

3.3.2 Metal Oxides Promoters

ZrO_2 is considered as a promoter when added to the catalyst in small amounts and receives highest interest among the other metal oxides promoters. Therdthianwong [193] concluded that Ni/Al_2O_3 catalyst deactivation was inhibited by ZrO_2 addition. The ZrO_2 promoter enhanced dissociation of CO_2 forming oxygen intermediates near the contact between ZrO_2 and Ni, where coke deposits were gasified afterwards. It was also shown that the method of catalyst preparation in the presence of ZrO_2 affected the catalyst texture and surface area due to the formation of ZrO_2–Al_2O_3 composites and the plugging of the Al_2O_3 pores by ZrO_2. As a result, the co-impregnated 15Ni/10% ZrO_2/Al_2O_3 catalyst had a higher BET surface area and activity than the sequentially impregnated catalyst.

Another example for promoters that inhibits metal reactivity [161] on γ- Al_2O_3 was obtained when activity and catalytic stability tests were done between alkali metal oxide (Na_2O), alkaline-earth metal oxides (MgO, CaO) and rare-earth metal oxides (La_2O_3, CeO_2) catalysts. From the obtained results, CaO, La_2O_3, CeO_2 > No Promoter > Na_2O and MgO, it can be learned that promoters can rather increase reactivity of carbon species toward CO product, or alternatively, can decrease reactivity due to blockage of Ni active sites.

In a similar study involving perovskite structure, Moradi [196] indicated that the partial substitution of Ni by Zn limits the migration of the active Ni. The $LaNi_{0.8}Zn_{0.2}O_3$ increased the

temperatures of reduction peaks, leading to more stable perovskite structure in comparison to the non-promoted $LaNiO_3$ structure.

3.3.3 Lanthanides and Potassium Promoters

Amin findings [60] showed that the addition of lanthanides [197] (rare earth elements atomic numbers 57 through 71) promoters onto $Ni/\gamma-Al_2O_3$, resulted in relatively small pore sizes of the promoted catalysts support leading to a low product conversions by the order of no promoter > Eu > Tb > Ho > Tm > Er > Dy > Pr > Sm > Gd > Nd. However, the promoted $Ni/\gamma-Al_2O_3$ catalysts exhibited a high stability due to the suppressing of the deposited coke.

Borowiecki *et al.* [198-200] proved that potassium has the ability to suppress the carbon formation on SMR process in which the reaction mechanism and kinetics are comparable to the DRM [201, 202]. It was shown that K enhances steam adsorption which also presents in DRM from the RWGS side reaction (Eq. 13). However, this promoter shown very limited enhancement where domination of K–Ni interaction appeared and thus it was necessary to apply a preparation method that will ensure the location of the K promoter exclusively on the surface of the Al_2O_3 support [198].

3.3.4 Summary of the Role of Promoters

Numerous studies performed comprehensive research on DRM by metal or metal oxide promoted catalysts as inhibitors for carbon formation. Studies showed the positive effect of using different combinations of the active metals-supports with promoters. The ratio of promoter to the active metal was shown to be as crucial as the reforming procedure for stable operation of the DRM. It was shown that the utilization of high ratios of promoter did not necessarily favor with the catalytic activity. Unlike active metal studies that clearly conclude which active metal perform best, an agreement of which promoter is the best does not exist and further studies have to be made in this field.

However, among the known studies today, catalysts that were tested at different thermodynamic conditions and flow rates mostly indicate two types of promoters that show remarkable high activity and stability. (i) Ni based $\gamma-Al_2O_3$ with a combination of Ce and Ca promoters over a ratio of 3%Ni+0.15%Ce+0.05%Ca [33] and (ii) a ZrO_2 promoted $15Ni/10\%ZrO_2/Al_2O_3$ which enhanced the dissociation of CO_2 forming oxygen intermediates that gasified the coke deposits.

3.4 Catalyst Preparation

Catalysts preparation methods have a strong influence on the catalyst final properties [203]. The reactivity of the catalyst largely depends on the nature and the concentration of the imperfections that can be generated during preparation. Preparation techniques and pretreatment processes such as precursor and solvent concentration, pH, calcination temperature and aging time affect the final catalyst structural properties and the reduction behavior which directly affect the catalytic performance.

In this chapter, the most often used catalysts preparation methods, *i.e.*, impregnation, co-precipitation and sol-gel will be discussed with some references and the comparisons with other related catalyst preparation methods for the DRM.

3.4.1 The Impregnation Method

The impregnation method is related to an ion-exchange and adsorption processes where the interaction with the support has major effect of catalysts property. Impregnation is the simplest method for supported catalysts preparation while electrostatic forces control the adsorption mechanism [204]. Impregnated catalysts for DRM are prepared by impregnating a metal salt on a porous support whereas the metal loading of the catalyst is typically 1−5 % [160]. The impregnation method offers three major catalyst structures [205-207]:

a. Egg-white (or uniform distribution).
   Achieved by weakly interacting precursors and relatively mild drying (Figure 7) [208].
b. Egg-shell.
   Presents strong adsorption during impregnation by viscous solution and slow drying regime [209].
c. Egg-yolk, fast drying regime.
   Achieved by inhibition the leaching solution to enter the core of the reduced homogeneous catalyst pellet (Figure 8).[208].
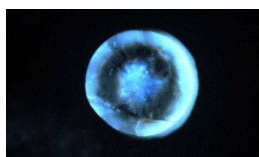

Fig. 7. Optical micrograph of egg-white type of Co/SiO_2-catalyst synthesized by leaching of a reduced shell-type of Co/SiO_2 catalyst pellet; Diameter of catalyst pellet: 2.5 mm.
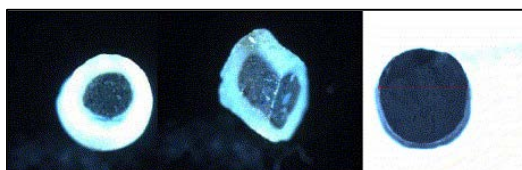
Fig. 8. Optical micrographs of egg-yolk type of Co/SiO$_2$-catalyst (left) synthesized by leaching of a reduced homogeneous catalyst pellet (right). Diameter of catalyst pellet: 2.5 mm.

Osama *et al.* [205] revealed successful selection of the impregnation method for the preparation of a Ce-promoted Ni/Al$_2$O$_3$ catalyst by the alkoxide method followed by reduction in a hydrogen stream. Similarly, Ren *et al.* [210] prepared Ni/SiO$_2$ from different sources by the incipient impregnation method and showed that the complexing agent and the selection of the impregnation method well affected the Ni/SiO$_2$ (i) surface area, (ii) size and dispersion of Ni, (iii) the reduction behavior, (vi) and the coking and sintering resistance of the catalyst.

Albarazi *et al.* [211] proved that the synthesis route has a marked influence on the physic-chemical features of the catalyst by the preparation of Ni/SBA-15 catalysts through impregnation, as well as by co-precipitation. Pore blockage was observed in the catalyst that was prepared by co-precipitation. NiO particles with crystal sizes of 9-11 nm were observed outside the mesoporous structure of the SBA-15 support in the case of the catalysts prepared by impregnation [211]. An important catalytic characteristic was achieved by the presence of the NiO species which result in slightly lower catalytic activity but also improved stability and resistance towards methane decomposition (Eq. 11).

3.4.2   The Precipitation and Co-Precipitation Methods

Precipitation is a process in which a phase-separated solid is formed from homogeneous solution. This method is one of the most widely employed preparation methods and used to prepare both single component catalysts and catalyst supports such as Al$_2$O$_3$, SiO$_2$, TiO$_2$ and ZrO$_2$ [212]. Solids crystallization over precipitation method typically occurs at relatively low supersaturation, which is induced mostly by solution temperature increase and solvent evaporation [213, 214]. The solid is achieved by the formation of mixed crystals through adsorption, occlusion and/or mechanical entrapment when the solution is supersaturated with the precipitated macrocomponent [215].

Bimetallic catalysts for DRM are prepared by the co-precipitation method (simultaneous precipitation of more than one component). During co-precipitation the pH has to be adjusted for the non-solubility of the precursors and hydroxides are the preferred precipitates due to their low solubility, easy decomposition and minimal toxicity and environmental problems. In similarity to the precipitation method, the involved materials in the co-precipitation method are subjected to calcination, reduction, and passivation [216].

Cavani [217] showed that in order to form bimetallic catalyst, the addition of sodium hydroxide (NaOH) to a non-soluble compounds such as Ni hydroxide Ni(OH)$_2$ and cobalt hydroxide Co(OH)$_2$ increase the basicity, resulting in that compounds that are usually not soluble in water can be solute [212]. The same method was successfully utilized by Martínez *et al.* [218], Zhang [77] and Benrabaa [219] for the preparation of Ni–Me (Me = Co, Fe, Cu, or Mn) catalysts.

The co-precipitation is also used when both metal and support are being precipitated stimulatingly as presented by Pennina [220] and Zanganeh *et al.* [221] for the simultaneous preparation of monometallic crystalline Ni/Al_2O_3 and NiO–MgO with the addition of surfactant.

Advanced precipitation methods, such as microemulsion synthesis tend to perform better in certain cases but do not yield catalysts with sufficiently superior quality to compensate for the higher cost involved [52, 222]. Hence, conventional precipitation and co-precipitation from aqueous solution will most likely continue to be one of the preferred methods of catalyst synthesis in the next years [223].

A comparison between impregnation and precipitation methods has shown numerous advantages of the former one:

(a) The pellets are shaped before the metal is added.
(b) The filtering and the wash of the catalyst are eliminated.
(c) Small metal loadings are easily prepared.
(d) Impregnation offers some control over the distribution of the metal in pellets.

However, compared to the precipitation, there are also associated disadvantages for the impregnation:

(a) High metal loadings are not possible, maximum loading obtained is less than one monolayer.
(b) A good impregnation solution for a certain required process is difficult to achieve.

3.4.3 The Sol-Gel Method

Sol-gel methods have been recognized as very effective procedures to immobilize the metal precursors on the mesoporous support to prepare catalysts for the DRM [224]. The versatility of the sol-gel techniques allows control of the texture, composition, homogeneity and structural properties of solids and promote metals dispersion. The sol-gel method cannot be defined as a single technique since a broad variety of procedures exist with similar order of preparation steps [225]:

(a) Conversion of dissolved molecular precursors to the reactive state.
(b) Polycondensation of activated molecular precursors into nanoclusters (formation of colloidal solution)
(c) Gelation
(d) Aging
(e) Washing
(f) Drying/Stabilization.

Zhang *et al.* [226] showed that the sol–gel technology was appropriate method to prepare a mixed-metal oxide catalysts. The sol–gel provided highly controllable preparation route with inherent advantages such as molecular-scale mixing of the constituents and homogeneity of the product. It was shown [226] that the fresh precipitate produced from the hydrolysis of either alkoxide or inorganic salt could be peptized with acid to yield a stable colloidal solution (or sol) under appropriate conditions. The use of inorganic salt precursor rather than organic alkoxide precursor can not only reduce the cost of synthesis, but also avoid the use of organic solvent to decrease pollution.

Sol–gel is different from precipitation synthesis being that in a sol–gel method, the formed solid is a container spanning hydro or alcogel, while in the precipitation method a clear phase separation occurs. However, often a sol–gel synthesis is referred to cases where alkoxide precursors are used, regardless of whether a true gel is formed as an intermediate, or a precipitate with clear phase separation occurs.

3.4.4   The Polyol and Surfactant-Assisted Methods

Naeem [227] prepared Ni-based nanocatalysts by two methods: Polyol (an alcohol containing multiple hydroxyl groups) and CTAB (cetyl trimethyl ammonium bromide) surfactant-assisted. Over similar reaction conditions, polyol catalysts exhibited the highest activity and selectivity, whereas the surfactant-assisted catalysts showed minimum carbon deposition. CO_2-TPD and H_2-TPR revealed that the preparation method had a significant effect on the basicity and reduction behavior of prepared catalysts. In the case of surfactant-assisted catalysts, the high basicity was their prime characteristic that made them better coke-resistant. It can be concluded that both preparation methods exhibited good potential to be used as catalysts preparation methods for DRM.

3.4.5   Advanced Preparation Methods

3.4.5.1   The Improved Co-Precipitation/Reflux Digestion Method

An improved co-precipitation method was presented by Zhang *et al.* [228] for the preparation of mesoporous amorphous Ni–ZrO_2 catalysts with prolonged reflux digestion. This advanced method introduced the "anchoring effect" which afforded the synthesis of highly dispersed Ni nanoparticles in a mesoporous amorphous matrix, exhibiting excellent activity and thermal stability at elevated temperatures in comparison to the catalyst that were prepared by conventional impregnation and co-precipitation methods. Catalysts exhibited superior activity, however, long-term stability and high carbon deposition resistance for this method was not proven.

3.4.5.2 The Impregnation with Non-Thermal Plasma

Rahemi *et al.* synthesized Ni/Al$_2$O$_3$–ZrO$_2$ nanocatalysts [166] via impregnation and non-thermal plasma treatment. The results showed that the plasma treatment produced highly dispersed nanoparticles with high surface area and strong interaction between the active phase and the support. The small Ni particles over the plasma-treated Ni/Al$_2$O$_3$–ZrO$_2$ nanocatalyst lead to a better catalytic activity and better coke inhibition.

Although preparation of heterogeneous DRM catalysts with different methods have been investigated extensively, new challenges still appear continuously, which necessitates the continuous focus on the improvement of tailored catalysts for DRM commercializing. More broadly, despite the fact that the synthetic methodology is already well defined, the realization to obtain the exact structure, morphology and function of the produced products is still hard to achieve which drives the further investigation specifically focused on more controllable synthesis.

3.5 Catalysts Characterization

Despite the fact that DRM has not been industrialized yet there is still a remarkable development of catalysts for this process. Catalyst development progress is directly connected to the improvement of catalyst characterization techniques. Advanced characterization technics provides the ability to enhance the catalytic processes by accurate determination of the fine differences between catalyst physical and chemical properties. Characterization methods can figure the thermodynamic effect *in situ* in order to track the root cause for catalyst deactivation and to determine what inhibition methods are mostly suitable to be used.

Catalysts characterization involves two main categories (i) the investigation of the physical properties over the porous nature of the catalyst, made by physical analysis methods and (ii) chemical investigation on the active sites properties that are dispersed on the support surface.

3.5.1 Physical Analysis Characterizations

3.5.1.1 Surface Area and Porosity

High surface area, pore volume and pore diameter are important physical properties that strongly influent the catalytic performance and therefore it is important to determine and control these characteristics. A typical expected porosity values for a mesoporous γ- Al_2O_3 catalyst support for the DRM will be 50-400 m^2/gr, typical pore diameter is 9-21 nm and a typical BJH (Barrett-Joiner Halenda procedure [229]) pore volume is 0.8-2.0 cm^3/g [157].

The specific surface area of a catalyst is estimated from the amount of nitrogen adsorbed on the catalyst surface in relationship with its pressure at the boiling temperature of liquid nitrogen under normal atmospheric pressure. The catalyst porosity and surface area are characterized by adsorption isotherms, interpreted through the BET model.

3.5.1.2 Scanning Electron Microscopy (SEM)

The SEM uses a focused beam of high-energy electrons to generate a variety of signals at the catalyst surface. The signals (derived from electron-sample interactions) reveal information about the sample including external morphology (texture), chemical composition, and crystalline structure and orientation of materials making up the sample. The data is collected over a selected area of the sample surface and a two dimensional image is generated and displays spatial variations in these properties. Areas ranging from approximately 1 cm to 5 microns in width can be imaged in a scanning mode using conventional SEM techniques [230].

Figure 9 below shows SEM images over micrometer scale to demonstrate the effect of K promoter on carbon deposition over Ni/Al$_2$O$_3$ catalyst, the comparison confirms that a lower amount of coke was deposited on sample B with higher K content.
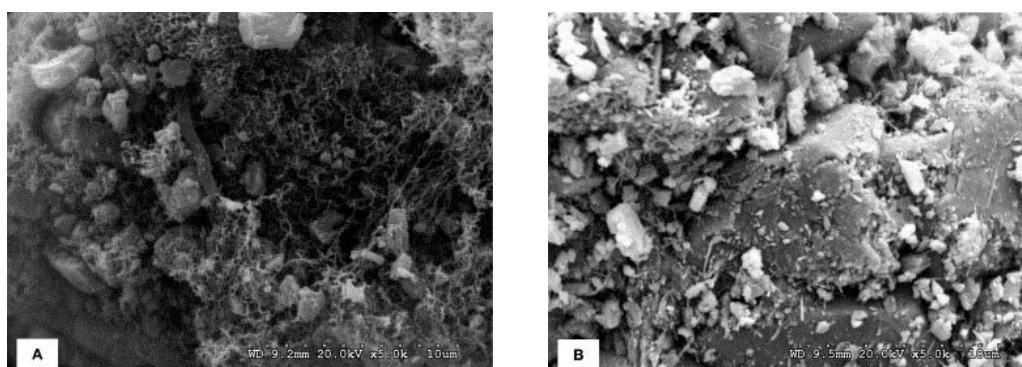

Fig. 9. SEM images shows lower coke deposition on sample B.

3.5.1.3 Transmission Electron Microscopy (TEM)

The TEM method yields information on the internal structure of materials using electromagnetic lenses to focus magnified images onto phosphorescent screens or digital cameras. TEM may require preparation of a sample film or section no thicker than 60-80 nm, through which the electron beam is transmitted. At a maximum potential magnification of 1 nanometer, the TEM images utilizes energetic electrons providing a morphologic, compositional and crystallographic information and is considered as ideal for metallurgy analysis[230]. Figure 10 below shows TEM images over nanometer scales to demonstrate the effect of K promoter on carbon deposition over Ni/Al$_2$O$_3$ catalyst. The comparison confirms that a lower amount of coke was deposited on sample B with higher K content
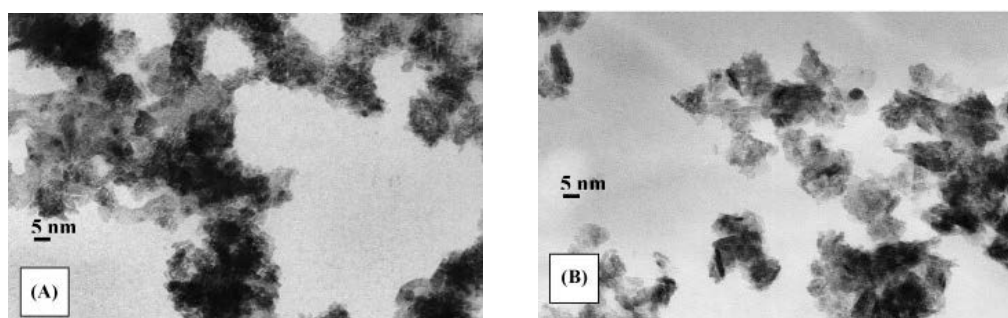

Fig. 10. TEM images shows lower coke deposition on sample B.

3.5.1.4 Powder X-ray diffraction

X-ray diffraction (XRD analysis or XRPD analysis) is a method for crystallinity determination. The result from an XRD analysis is a "diffractogram" showing the intensity as a function of the diffraction angles. Positive determination of a material using XRD analysis is based on

46

accordance between the diffraction angles of a reference material and the catalyst sample. The x-ray diffraction pattern generated in a typical XRD analysis, provides a unique "fingerprint" of the crystals present in the sample catalyst. When interpreted by comparison with standard reference patterns and measurements, this fingerprint allows identification of the crystalline form and by that, confirmation that the checked material is indeed the desired one.

3.5.1.5 X-ray Photoelectron Spectroscopy

X-ray photoelectron Spectroscopy (XPS) for chemical analysis is widely used surface analysis technique as it can be applied to a broad range of catalysts and provides valuable quantitative and chemical state information from the surface of the catalyst to determine the formation or the changing of chemical states in the spent catalysts, compared to the fresh catalyst just after reduction. The average depth of analysis for an XPS measurement is 5 nm. The XPS instruments function in a manner analogous to SEM instruments by using a finely focused electron beam to create SEM images for sample viewing and point spectra or images for compositional analysis. Laosiripojana *et al.* [233] used the XPS measurement to show that Ce^{3+}/Ce^{4+} ratio over CeO_2 doped Ni/Al_2O_3 after reduction was 0 and raised to 0.21 after exposure in DRM conditions.

3.5.2 Chemical Characterization of the Active Sites

3.5.2.1 TPR, TPD and TPO Analyses

TPR is used for the characterization of metal oxides, mixed metal oxides, and metal oxides dispersed on a support. The TPR method yields quantitative information of the reducibility of the oxide's surface, as well as the heterogeneity of the reducible surface. By performing TPR, the analyzer determines the number of reducible species present in the catalyst and reveals the temperature at which the reduction occurs.

The TPR analysis begins by flowing analysis gas (typically hydrogen in a nitrogen or argon as the inert carrier gas) through the sample, usually at ambient temperature. While the gas is flowing, the temperature of the sample is increased linearly with time and the consumption of hydrogen by adsorption/reaction is monitored. Changes in the concentration of the gas mixture are determined. This information yields the hydrogen uptake volume.

Castro *et al.* [232] checked the influence of K, Sn, Mn and Ca on the behavior of a Ni-Al_2O_3 catalyst and used the TPR method to evaluate the minimal reduction temperature of the modified catalysts. Utilization of the TPR revealed that The Ni catalyst show a unique band between 590 and 900 °C with a maximum located at about 825 °C (Figure 11).
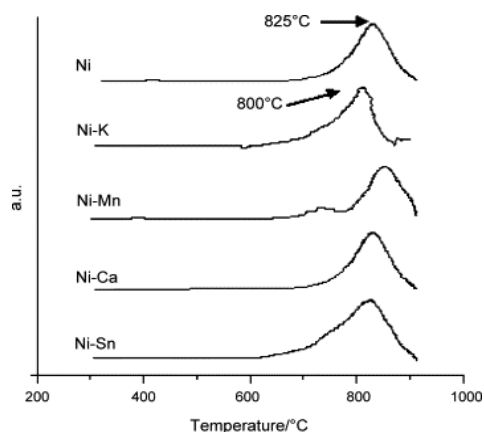
Fig. 11. TPR curves, 5% H_2 in N_2, 30 ml min^{-1}, 283 °K min^{-1}).

Temperature-Programmed Desorption (TPD) determine the number, type, and strength of active sites available on the surface of a catalyst from measurement of the amount of gas desorbed at various temperatures. After the sample has been outgassed, reduced, or otherwise prepared, a steady stream of analysis gas flows through the sample and adsorbs on the active sites. TPD begins by increasing the temperature linearly with time while a steady stream of inert carrier gas flows through the sample. At a certain temperature, the heat overcomes the activation energy; therefore, the bond between the adsorbate and adsorbent will break, and the adsorbed species desorb. If different active metals are present, they usually desorb the adsorbed species at different temperatures. These desorbed molecules enter the stream of inert carrier gas and are swept to the detector, which measures the gas concentrations. The volume of desorbed species, combined with the stoichiometry factor and the temperature at which pre-adsorbed species desorb, yields the number and strength of active sites.

Temperature-Programmed Oxidation (TPO) examines the extent to which a catalyst can be oxidized or was previously reduced. Usually the sample is pretreated and the metal oxides are reduced to the base metal, typically with a gas mixture of hydrogen with either nitrogen or argon. Then the reactant gas, typically 2-5% oxygen with helium, is applied to the sample in pulses or, alternatively, as a steady stream. The furnace heats the sample tube and sample according to the selected temperature program and the oxidation reaction occurs at a specific temperature and the instrument measures the uptake of oxygen.

Regardless of which experiment type is performed using a TPX instrument, the basic concept uses filament that detects changes (thermal conductivity) in the gas mixture flowing through it *in situ*. The sample, the gas selection, and the analysis conditions determine what changes occur [231].

3.5.2.2 Pulse Chemisorption Analysis

The pulse chemisorption analysis determines active surface area, percent metal dispersion, and the average active particle size by applying measured doses of reactant gas to the sample.

48

The gas reacts with each active site until all sites have reacted. Once the active sites have completely reacted, the discretely injected gas volumes elute from the sample tube unchanged. The amount chemisorbed is the difference between the total amount of reactant gas injected and the amount that eluted from the sample.

3.5.3   Complementary Set of Characterization Methods

In order to understand and develop the catalysts and their supports, numerous physical and chemical properties must be characterized in order to obtain a clear understanding of the catalyst functions and link the catalyst properties to the activity, selectivity, and/or deactivation mechanisms. An example for complementary set of characterization methods that was used by Djaidja [234] and by Therdthianwong [235] to determine the characteristics of the supported catalyst for DRM experiment includes BET, H_2-TPR, TPO, XRD, and TEM.

4 THERMODYNAMICS AND KINETICS OF METHANE DRY REFORMING

4.1 Thermodynamics Fundamentals

DRM is an endothermic process (Eq. 1). The requirements for high external heat supply and slow reactions that involve long conversion times [236] keep the DRM process far from industrial use [237]. In order to industrialize the DRM process, mitigating of the difficulties is required by utilization of advanced reforming techniques. Furthermore, a critical problem over the DRM process is the rapid carbon deposition. Carbon deposition is significantly affected by the process thermodynamics and likely to occur by two side reactions (i) the methane decomposition (Eq. 11) and (ii) the Boudouard reaction (Eq. 12). These reactions lead to catalyst deactivation by the blockage of the catalyst active sites and can also block the reactor in industry applications.

DRM studies show that the thermodynamic equilibrium fundamentals are interconnected to the kinetic mechanisms and it plays an important role for efficient process control, both from energy/cost considerations and catalyst deactivation inhibition methods. In general, it can be defined that the thermodynamics determine "if reaction will occur" and kinetics determine "how it will occur".

4.2 Thermodynamic Aspects of DRM and the Associated Side Reactions

DRM reactions (Eq. 1-4) are facilitated by heterogeneous catalyst, allowing reactions to proceed on a different reaction pathway. The different pathway involves a lower-energy transition state and allows the system to reach equilibrium faster for both the forward and reverse reaction rates equally. However the addition of a catalyst has no effect on the final equilibrium of the reaction which is ruled by the thermodynamic variables. In fact, catalysts affect the kinetics, but does not affect the thermodynamics.

A thermodynamically favorable reaction is when Gibbs free energy is negative ($\Delta G < 0$). Studies of thermodynamics equilibrium [238] are usually done by the ΔG minimization method to understand and optimize the DRM variables combinations such as temperature, pressure and different feed product ratios.

The relation between the thermodynamics and the kinetics is expressed when examining the effect of reactants ratio (CO_2/CH_4) on the thermodynamic equilibrium and on the partial pressure reaction rates that are determined through activation energy value on the Arrhenius equation.

DRM main reaction (Eq. 1) is favored by low pressure as seen in the stoichiometry of the reaction but requires high temperature as shown in ΔG (Eq. 1). The main reaction is followed by side reactions (Eq. 2-4) while two of them are directly related to carbon deposition.

The methane decomposition (Eq. 11) is an important source of carbon deposition. Similar to the main reaction, the ΔG^0 is reduced with increasing temperature making this reaction thermodynamically more favorable. The Boudouard Reaction (Eq. 12), in similarity to Eq. (2), is responsible for carbon deposition but in contrary to Eq. (11) it is favorable with temperature increase as seen from its ΔG° Eq. (12). The RWGS side reaction (Eq. 13) and its ΔG^0 equation shows that high temperatures make this reaction as unfavorable and less H_2O will be produced.

The ΔG^0 change is employed not only to define the minimum operating temperatures of the main reaction but also for the minimization of the methane decomposition Eq. (11). ΔG^0 is also used for the calculation of limiting temperatures that turn it to positive value and favor with the Boudouard reaction Eq. (12) and the water gas shift Eq. (13).

4.3   The Effect of Pressure

Stoichiometric shows that for DRM, CO_2 and CH_4 conversions are higher at lower pressures than those at higher pressures [98]. This fact suggests that at high temperature, greater pressures can suppress the temperature effect on the increasing reactant conversion. These decreased trends can be expressed by endothermic properties of the DRM, which tends to shift to the reactant side (LeChatelier's principles) [239]. Besides, methane decomposition (Eq. 11) and Boudouard reaction (Eq. 12) contribute in lowering CH_4 and CO_2 conversions, as well as decreasing CO and H_2 formation at the higher pressures. Nikoo *et al.* [98] thermodynamically calculated that for reactions at 1173 K, H_2O that is originated from RWGS (Eq. 13) disappears at 1 bar, but increases along with the pressure. Contrary to previous studies [240] [241] which did not consider solid carbon in the equilibrium reaction system, the presence of solid carbon in this thermodynamic equilibrium resulted in greater moles of H_2 than those of CO within the whole investigated range of pressure and led to $H_2/CO > 1$.

Johnson [242] performed thermodynamic calculations on the CO disproportionation (Eq. 12) and methane decomposition (Eq. 11) over Ni , Pt , and Rh supported catalysts at 1073 °K at a pressure range of 1-14 bar. The amount of carbon deposited on Pt and Rh-supported catalysts at 1 bar were much less compared to that produced at 14 bar. At low pressure, CO_2 appeared to be the major source of carbon deposited onto these catalysts. This finding is in agreement with Tsipouriari *et al.* for Rh supported catalyst [243]. However, at 14 bar and on the Ni-supported catalysts the deposited carbon comes from both methane and CO_2, depending on reactant partial pressure. It can be concluded that the carbon deposited by methane decomposition reaction (Eq. 11) decreased with increasing pressure, while simultaneously the CO disproportionation reaction (Eq. 12) was enhanced. These results suggest that CO disproportionation reaction (Eq. 12) is the most favorable factor to carbon formation at a higher pressures, particularly when the CO_2/CH_4 ratio is higher than unity. However, due to the CO disproportionation reaction (Eq. 12), CO decreases with a steeper slope than H_2 when increasing the pressure. These results that fit the thermodynamic calculations are consistent with the conclusion that the CO disproportionation (Eq. 12) is the main route for carbon formation in DRM.

Istadi [244] also checked the effect of system pressure at 1123 °K and CO_2/CH_4 over unity feed ratio and in agreement with Nikoo *et al.* [98], showed that the main DRM reaction and the RWGS (Eq. 13) show a positive stoichiometric value. As presented in Figure 12 increasing the system pressure decreases the mole fractions of both products at equilibrium. Similar trend appears in Figure 13 which corresponds to lower H_2 and CO selectivity with system pressure.
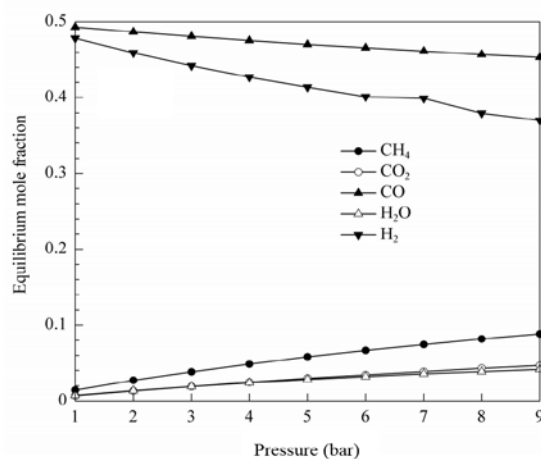

Fig. 12. Effect of system pressure on equilibrium mole fractions of products at CO_2/CH_4 with feed ratio 1 for CH_4, CO_2, CO, H_2O and H_2 at temperature 1123 °K [244].
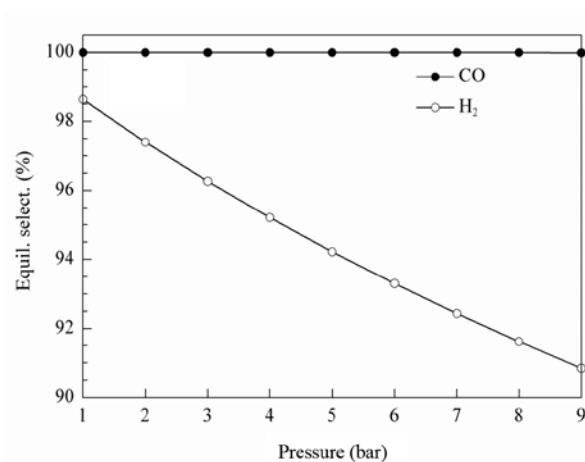
Fig. 13. Effect of system pressure on equilibrium selectivity % of H_2 and CO products at temperature 1123 °K and CO_2/CH_4 feed ratio 1 [244].

The effect of system pressure on the equilibrium conversions is displayed in Figure 14. The equilibrium conversions of CH_4 and CO_2 decrease with increasing system pressure. As expected, the reaction shifted to the reactant side and decreased the reaction due to positive and/or zero stoichiometric of all reactions considered in the DRM.
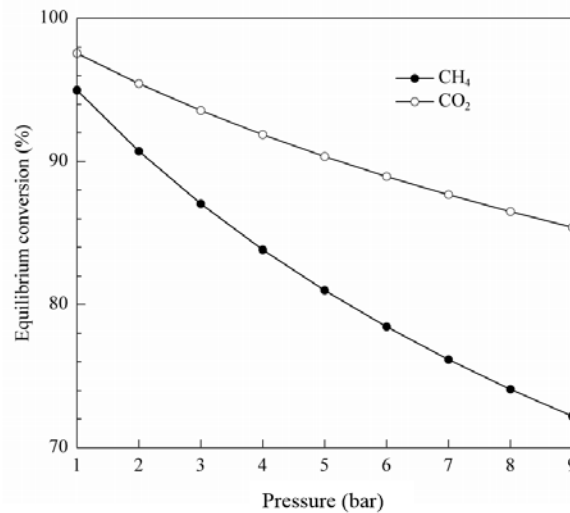
Fig. 14. Effect of system pressure on equilibrium conversions % of CH_4 and CO_2 at temperature 1123 K and CO_2/CH_4 feed ratio 1[244].

As presented by Wang *et al.* [245] and Istadi [244], the using of Ni based catalyst, at low pressure of 0.01 bar leads to conversions of 90% at 550 °C while at 0.1 bar, the conversion does not reach 90% until 700 °C. It can be concluded that carbon deposition resulted from CO disproportionation (Eq. 12) is thermodynamically favored at higher pressures, however, carbon deposition caused by methane decomposition is thermodynamically favored at lower pressures [109].

When temperature is fixed, reactants conversions at lower pressures are always higher than those at higher total pressures as derived from the stoichiometry of the main reaction. In general, reaction temperatures above 1100 °K and CO_2/CH_4 ratio=1 are favorable for syngas production with H_2/CO ratio close to unity. This product ratio is favored as feed stock ratio for the F-T synthesis [194].

4.4 The Effect of Temperature

4.4.1 CH₄ Conversion

Operating temperatures at 1 bar affect the equilibrium state in a way that for all CO_2/CH_4 ratios, CH_4 conversion increases with temperature up to 1073 K. This fact indicates that the CO_2 gas has a positive effect as a soft oxidant on CH_4 conversion with temperature increase.

Thermodynamic calculations made by Nikoo *et al.* [98] showed that the positive effect on reactant conversion is noticeable at temperatures lower than 973 °K. Therefore the addition of CO_2 to CH_4 as an active oxidant provides higher activity for methane molecules. Nevertheless, the exothermic side reactions are involved in decreasing methane conversion at the lower temperatures. Nikoo *et al.* [98] predicted for the equilibrium conversion rate was about 82% for

CO_2/CH_4 ratio of unity and temperature of 873 °K, considering that methane decomposition (Eq. 11) lays the foundation of methane conversion. In contrast, Istady [244] calculated 42% conversion for similar conditions. Figure 15 presents the calculated CH_4 equilibrium conversion as a function of temperature and CO_2/CH_4 different ratios at 1 bar for $n_{(CH4 + CO2)} = 2$ mol. Khalesi *et al.* [246] experimentally confirmed Nikoo *et al.* [98] calculations. In addition it was shown that for temperatures higher than 923 °K the presence of promoted Ni based catalyst led to higher CH_4 conversion due to the lower sensitivity of the catalyst to carbon deposition at higher temperatures.
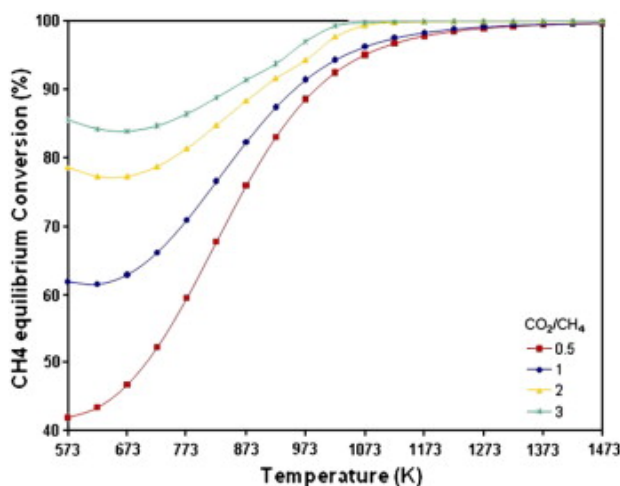

Fig. 15. CH_4 equilibrium conversion as a function of temperature and CO_2/CH_4 ratio at 1 bar for n $_{(CH4 + CO2)}$ = 2 mol.

It can be concluded that temperature favors CH_4 conversions up to certain limit, whereas this limit can be increased if advanced process technology is integrated.

4.4.2 CO_2 Conversion

Conversion of CO_2 is important since CO_2 as a necessary oxidant has a positive effect on CH_4 conversion and acts differently from CH_4 which thermodynamically increase conversions within temperature increase of for any CO_2/CH_4 ratios.

Nikoo's [98] calculations for CO_2 conversion depicted two trends of conversion *vs.* temperature for any CO_2/CH_4 ratios as seen in Figure 16 (CO_2 equilibrium conversion as a function of temperature and CO_2/CH_4 ratio). CO_2 conversion gradually decreases with temperature starting at 573 K with CO_2/CH_4 ratios variations of 0.5-3, down to 60%-15% respectively and then increases back at about 823–873 °K up to 100% conversion. CO_2 conversion reaches a maximum between 1273 °K and 1473 °K for any CO_2/CH_4 ratio. Istady [244] experimentally showed that CO_2 is completely converted at CO_2/CH_4 ratio of 0.5 and temperature of 1273 °K better than CO_2/CH_4 on larger proportion. This total CO_2 consumption in low ratios is due to the fact that it functions as the limiting reactant in the reaction.

The first decreasing trend can be mainly described by the RWGS reaction (Eq. 13), which converts CO_2 and H_2 to a large quantity of carbon and water. This exothermic reaction spontaneously occurs at the low temperature, but diminishes as the equilibrium constant decreases and reduces CO_2 conversion as shown in $\Delta G°$ of RWGS reaction (Eq. 13). This trend can also be verified by decreasing moles of H_2O in the mentioned temperature range. The other side reactions are not involved in CO_2 conversion, as they have a negative value of Ln (K) (inversed Arrhenius Form, Eq. 5) within the mentioned temperature range. Whenever the CO_2/CH_4 ratio is greater, CO_2 conversion is lower, as CH_4 more intensively plays the role of a limiting reactant, concerning that at CO_2/CH_4 ratios higher than unity, the equilibrium conversion of CO_2 cannot be completed. These results are in agreement with Wisniewski *et al.* [247] observations on DRM over Ce promoted Fe based catalyst in which conversions of CO_2 exceeded to those of CH_4 lead to a very limited carbon deposition.
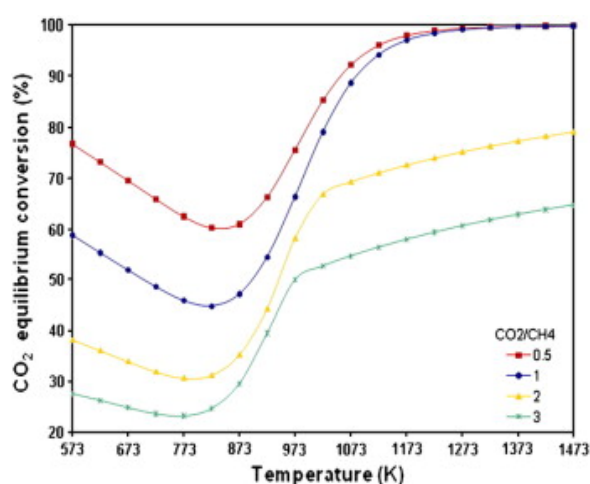

Fig. 16. CO_2 equilibrium conversion as a function of temperature and CO_2/CH_4 ratio at 1 bar for n $_{(CH4 + CO2)}$ = 2 mol.

As a conclusion, CO_2 plays the oxygen supplier role and the double trend caused not because of not being consumed but due to the fact that the RWGS (Eq. 13) that produce CO_2 is not favorable with high temperature.

4.4.3 H_2 Production

As shown in Figure 17, the region for H_2 production with respect to CO_2/CH_4 ratio is divided to: $CO_2/CH_4 > 1$ and $CO_2/CH_4 < 1$. Nikoo *et al.* [98] depicted that at 1 bar, the production of H_2 gas as a function of different temperatures and CO_2/CH_4 ratios < 1, enhanced for whole temperature range 573-1473 °K, since CO_2 is the limiting reactant and the RWGS reaction is not favored along with reaction due to the lack of CO_2 source [248]. However, the number of H_2 moles produced decreased with increasing CO_2/CH_4 ratio from 0.5 to 1 for all temperature range due to the fact that the main reaction is enhanced and suppressing the methane decomposition (Eq. 11) to produce H_2. For CO_2/CH_4 ratios > 1, the amount of produced H_2 increased along with temperature, attaining a maximum around 973–1023 °K, and then

55

reduced for higher temperatures. This decrease, for any CO_2/CH_4 higher than 1 is expected since RWGS reaction (Eq. 13) is increased due to higher CO_2 supply and lack of CH_4 supply, and the consumption of H_2 to produce more CO. This result is compatible with the thermodynamic analysis of Istadi [249], Yanbing [248] and Takano [250] who investigated the H_2 production from Ni/Al_2O_3 at 1000 °K onto DRM over different reactant ratios up to 3.
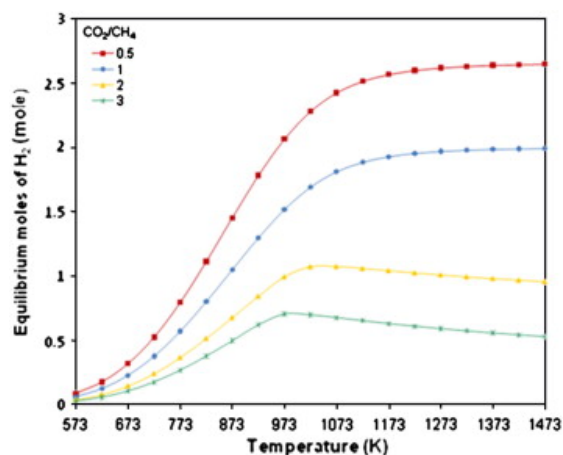

Fig. 17. Moles of H_2 as a function of temperature and CO_2/CH_4 ratio at 1 bar for $n_{(CH4 + CO2)}$ = 2 mol.

4.4.4 CO Production

Figure 18 shows the number of CO moles vs. CO_2/CH_4 ratio and temperature range of 573-1473 °K at 1 bar. It can be observed that higher temperatures favor CO production for any CO_2/CH_4 ratios, since all the reactions involved in CO production are endothermic [245]. At CO_2/CH_4 ratio < 1, CO production enhances along with increasing CO_2/CH_4 ratio. At 1173 °K the CO production of CO_2/CH_4 ratio =0.5 reach 1.3 moles and doesn't increase. The reason for the asymptotic behavior is that the CO_2 is the limiting reactant and although being favored, the CO lack of C source in order to be produced [245].

Highest CO production is obtained when CO_2/CH_4 ratio is in unity, however, increasing CO_2/CH_4 ratio > 1 at higher temperatures causes a decrease in CO production. An explanation for this performance is that the CH_4 becomes the limiting reactant for the main DRM reaction. This observation is consistent with the previous mentioned Takano [250] based on Ni/Al_2O_3 at 1073 °K. From the thermodynamic and stoichiometric point of view, CO production is favorable at the mentioned temperature range due to RWGS reaction where H_2 reacts with CO_2 to produce CO. This is in contrary to the decreasing trend of H_2 production for CO_2/CH_4 greater than unity versus temperature greater than 973 °K [227].

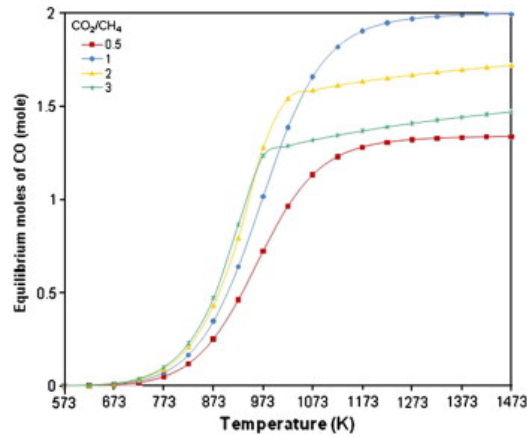Fig. 18. Moles of CO as a function of temperature and CO_2/CH_4 ratio at 1 bar for $n_{(CH4 + CO2)}$ = 2 mol.

An important value, derived from the results of the H_2 and the CO production is the products (H_2/CO) ratios that subsequently becomes the feed stock for the GTL process [12]. The H_2/CO ratio produced as a function of temperature and CO_2/CH_4 ratio at 1 bar are presented in Figure 19. It can be observed that the product ratio decreases with increasing both temperature and reactant ratio and becomes very low at temperature above 873 °K. This ratio fit better for industrial implementation, and the value close to unity is desired for the F-T process [251]. Figure 19 also shows that a H_2/CO ratio in the order of unity can be obtained at temperatures higher than 1173 °K for CO_2/CH_4 ratio in unity at which about 4 mol of syngas can be produced from 2 mol of DRM reactants with a CO_2 conversion of more than 98%.
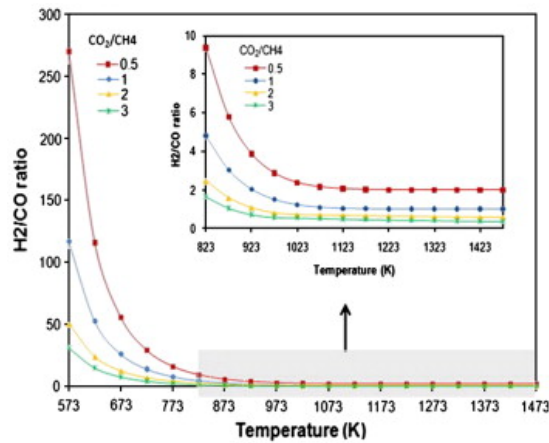

Fig. 19. H_2/CO ratio as a function of temperature (573–1473 K) and CO_2/CH_4 ratio at 1 bar for $n_{(CH4 + CO2)}$ = 2 mol.

In agreement with Nikoo *et al.* [98], Khalesi *et al.* [246] experimentally showed that good reforming performance (activity and stability) with product ratio close to unity and temperature range of 900-1073 °K at 1 bar can be achieved by using Ca-Sr promoted Ni catalyst over mixed Perovskite oxides. However, the energy saving by utilizing the lower temperature limit may lead to disadvantage since at lower temperatures more carbon is formed due to the thermodynamically favored methane decomposition (Eq. 11).

The conclusion from the above analysis is that in order to achieve product ratios close to unity that are desirable for F-T process, high temperatures and high reactants ratio are required. However, it should be noted that high temperatures may favor catalyst deactivation due to metal sintering and a proper consideration of the promoted active metal properties has to be taken.

4.4.5   Carbon Production

The reactions that are involved in carbon formation are affected by temperature and reactant ratio (Figure 20) due to their low equilibrium constants. It can be observed that carbon formation decreases with increasing temperature which functions as a barrier for the exothermic Boudouard reaction (Eq. 12). However, thermodynamic calculations [98] show that a considerable and nearly constant amount of carbon still remain for CO_2/CH_4 ~0.5 at temperatures higher than 1073 °K since temperatures become more thermodynamically favorable with the methane decomposition (Eq. 11). Similarly, Shamsi [242] showed that by the reverse Boudouard reaction (Eq. 12) which is thermodynamically favorable at the higher temperature especially for $CO_2/CH_4 > 1$ the carbon deposition rate is reduced. A singularity of carbon deposition increase was predicted [98] at CO_2/CH_4 ratio of 0.5 at temperatures less than 723 °K. The explanation for that is the RWGS (Eq. 13) is not plausible when CO_2 is the limiting reactant. This fact promotes the methane decomposition reaction (Eq. 11) due to the excessive CH_4 presence in the reaction.
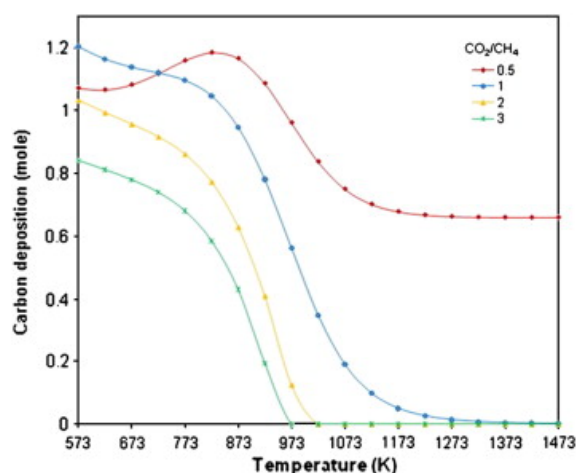

Fig. 20. Moles of carbon as a function of temperature and CO_2/CH_4 ratio at 1 bar for $n_{(CH_4 + CO_2)}$ =2 mol.

In general, carbon formation is expected to decrease with increasing CO_2/CH_4 ratio to above unity at a constant temperature, since CH_4 becomes more intensively a limiting reactant and the H_2 amount for the reactions is limited. According to Figure 20, low amount of carbon will be formed, achieving a H_2/CO ratio of unity at temperature higher than 1173 K for feed ratio of unity. Choudhary et al. [252] confirmed the above by comparing the rate of carbon deposition over Ni based catalyst , Co based catalyst, or bimetallic noble containing catalysts at 1123 K with CO_2/CH_4 in ratio of unity. Wang et al. [245] showed that at a given

pressure, the temperature limit for carbon deposition increases as the CO_2/CH_4 feed ratio decreases. It is important since using excess CO_2 in the feed inhibits carbon formation at lower temperatures by providing the reaction with excessive oxidation.

Claridge [253] showed two different forms of carbon deposition over DRM process (shown as the darker spots in the TEM image, Figure 21) . On the encapsulated form (or Ni carbide) carbon is associated on the catalyst and grows up to a full active site encapsulation that stops the process. On the Whisker carbon mechanism the dissociated carbon grows and extended while keeping the Ni active site ahead and creating a carbon nanotube. However, no thermodynamic model can predict which type of carbon will be formed during the DRM and it is considered to be ruled by the catalyst/support characteristics and the interactions between them [253].
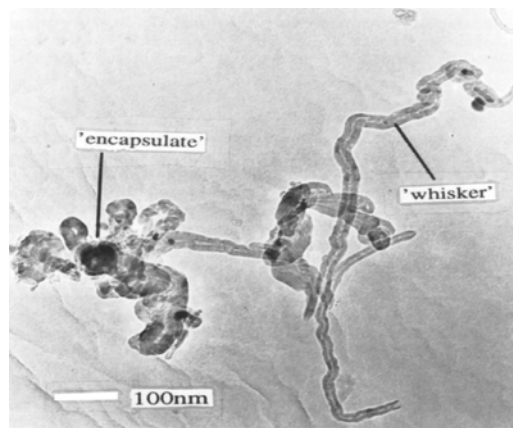

Fig. 21. Two different forms of deposited carbons: (i) the encapsulated Ni carbide and the (ii) whisker carbon. No thermodynamic model can predict which type will be formed during the DRM.

4.5 Summary of the Thermodynamic Effects

In conclusion, thermodynamic variables including temperature, pressure and reactant ratio have a wide range of effects on the reaction rate products distribution and by-product formation which are thoroughly described in the follow aspects:

a) The endothermic methane decomposition (Eq. 11) is the key reaction for carbon deposition when $CO_2/CH_4<1$, in high temperatures leads to constant moles of solid carbon and increased H_2 moles.

b) Water continuously forms in the reaction system by the RWGS reaction (Eq. 13) and its equilibrium concentration increases as the feed ratio increases and is reflected by lower hydrogen concentration than CO.

c) RWGS reaction (Eq. 13) is relatively not fast and active in low temperature and $CO_2/CH_4 < 1$, but favorable at temperature > 973 and CO_2/CH_4 ratio > 1 attested by the decreasing trend of H_2 production contrary to increasing trend of CO production within the mentioned ranges.

59

d) Optimal working condition for syngas with H_2/CO in the order of 1 can be formed at a temperature higher than 1173 K for CO_2/CH_4 ratio in unity.

e) CO_2/CH_4 ratio < 1 is favorable with the solid carbon formation within the entire considered temperature range.

f) The effect of high pressure on DRM revealed that methane decomposition (Eq. 11) and CO disproportionation (Eq. 12) result in low CH_4 and CO_2 conversions, as well as decreasing CO and H_2 formation.

g) For CO_2/CH_4 ratio > 1 at a higher pressures the disproportionation reaction (Eq. 12) is the most favorable contributor to carbon formation.

h) For CO_2/CH_4 ratio < 1 at a higher pressures the Methane Decomposition (Eq. 11) is the main contributor for carbon formation.

DRM thermodynamic equilibrium analysis uses the ΔG minimization methods to predict favorable reaction conditions. Thermodynamic analysis shows that the reaction temperature, pressure, and reactants (CO_2/CH_4) ratio significantly influence the reaction equilibrium, product composition and carbon formation.. In general, the DRM is favored with low pressures close to one bar, temperature range of 770-1170 °K and reactant ratio close to unity [201, 254, 255] while carbon deposition inhibition is considered as the main challenge for the research in this field.

4.6 Kinetics of the Dry Reforming of Methane

4.6.1 Kinetics and Reaction Mechanism, Governing Equations

Reversible reactions involve two reaction rate constants, the direct and the reverse, r_d and r_r respectively with corresponding activation energies that are determined through the k_0, the reaction rate constant. The Arrhenius form relates the thermodynamics to the kinetics and defines the equilibrium constant k (Eq. 5) that correlates the absolute temperature T and to the activation energy Ea while A is the pre-exponential factor and R is the universal gas constant.

Arrhenius Form:

$$k = Ae^{-\frac{Ea}{RT}} \tag{5}$$

Direct reaction rate constant:

$$r_d = kf(C_a, C_{b),} k = k_0 e^{-(\frac{Ea}{RT})} \tag{6}$$

Reverse reaction rate constant:

$$r_r = kf(C_R)k = k'_0 e^{-(\frac{Ea}{RT})} \tag{7}$$

Where C_X (x= a, b or R, Eq. 6, 7) is the component concentration and k is the rate factor as determined by Arrhenius Form.

The reaction equilibrium constant K (Eq. 8), will be expressed as the ratio of the above rates:

$$K = \frac{k_0}{k'_0} \tag{8}$$

The equilibrium constant K determines the extent in which the DRM reaction occurs [256]. The reactions cannot be shifted to the opposite side by changing the molar ratio of reactants when K is much higher than 1 [98], but for K in the vicinity of 1 varying the molar ratio of the reactants has considerable influence on the distribution of the products. Whenever ΔEa is negative on DRM, a larger Ln K indicates a spontaneous reaction is more feasible to occur.

From the equilibrium constant, based on the Arrhenius form and taking natural log of both sides of the equilibrium constant Eq. 9 is defined:

$$\Delta H = E - E' \tag{9}$$

This equation relates the enthalpy of the reaction with the direct and reverse activation energies and shows that for the DRM main reaction, the enthalpy $\Delta H > 0$ and, therefore, $E > E'$. Positive ΔH shows in similarity to ΔEa, that the direct reaction will be favored due to the lower activation energy.

Equations 5-9 shows the relation between the kinetics and the thermodynamics of the DRM process. The equilibrium constants that define the chemical reaction conversion are directly related to the ΔH through the activation energy Ea and affected by the reaction temperature T and the reactants partial concentration.

In general, there are different models to describe the reaction kinetics through different mechanisms [236]. In this work three models will be described while the power law kinetic model is considered to over simplify the mechanism and inaccurately predict the kinetic parameters the other two models are considered to be more comprehensive and comprise on a two different absorbance mechanisms.

4.6.2 The Power Law Kinetic Model

In general, this simple model provides a rough estimation of the parameters required and does not represent the kinetics of the reaction on a wide range of catalysts. The main advantage of the power-law models is the simplicity in application and parameter estimation such as the reaction order [40].

The power-law models calculate the kinetic rate for DRM reaction in the form of:

$$r = K[P_{CH_4}]^m \cdot K[P_{CO_2}]^n \qquad (10)$$

Where k is the power-law rate coefficient, m and n are the power constants for methane and the CO_2 partial pressure respectively. Bradford [240] utilized this kinetic model as an explanation to the experimental results for turnover frequencies of DRM over noble metal supported onto Al_2O_3 and TiO_2 support. This model confirmed that the turnover frequencies strongly depend on the space velocity and hence the percentage of equilibrium conversion. This model explained the need to work at low conversions relative to the equilibrium conversion in order to obtain an accurate kinetic data. In contrary to the above, Lyer et al. [241] showed that applying this model to predict and estimate the kinetics for DRM of cobalt based catalyst was insufficient and incapable of incorporating all of the mechanistic details involved in the reaction system. Similarly, Dong [257] and Akapan [258] used the power low model to serve as a starting point to assess the accuracy of empirical kinetic results and to evaluate mechanistic rate expressions and parameters, however, the power law model was too simple and was unable to predict the rate-determining step.

It can be concluded that the advantage of this model is the simplicity in application and determination. However, this model is insufficient over wide range of partial pressures and

cannot adequately explain the various reaction mechanistic steps which take place on the catalyst surface.

4.6.3 The Eley Rideal Model

The ER model (ER I and ER II, see below) for kinetic rate determination considers that only one of the reactants adsorbs onto the surface (reaction 1, Figure 22) and the other reactant interacts with the desorbed species on the gas phase, (reaction 2, Figure 22). it can be seen that higher coverage of the adsorbed species, as well as a higher pressure of the other gas, yields a higher reactions rate [41].
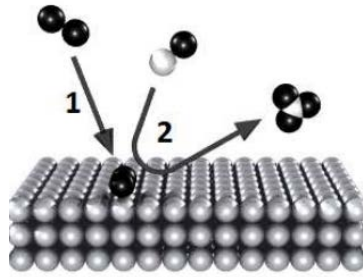

Fig. 22. The ER model, one of the reactants adsorbs onto the surface (reaction 1) followed by the desorption of the reaction products (reaction 2) [41].

The slow rate-determining step (RDS) is determined as the reaction of the adsorbed species with the other reactant from the gas phase leading directly to the products. The reaction rate for DRM is expressed as:

$$r_{Ref} = k_{Ref}\left(P_{CH_4} \cdot P_{CO_2} - \frac{P^2_{CO} \cdot P^2_{H_2}}{k_{Ref}}\right) \qquad (11)$$

As both reactants can theoretically be the adsorbed species, *i.e.* gaseous CO_2 reacting with adsorbed CH_4 or gaseous CH_4 reacting with adsorbed CO_2, both resulting ER I and II models can be considered,

ER I:

$$r_{Ref} = \frac{k_{Ref} \cdot k_{CH_4}\left(P_{CH_4} \cdot P_{CO_2} - \frac{P^2_{CO} \cdot P^2_{H_2}}{k_{Ref}}\right)}{1 + K_{CH_4} \cdot K_{CH_4}} \qquad (12)$$

ER II:

$$r_{Ref} = \frac{k_{Ref} \cdot k_{CO_2}\left(P_{CH_4} \cdot P_{CO_2} - \frac{P^2_{CO} \cdot P^2_{H_2}}{k_{Ref}}\right)}{1 + K_{CO_2} \cdot K_{CO_2}} \qquad (13)$$

63

Among the published literatures for ER models for DRM reaction, Akpan *et al.* [258] investigated the Ni/CeO₂–ZrO₂ catalyst. The kinetic model that best predicted the experimental rates was developed based on the ER model, assuming the methane dissociative adsorption was the RDS. The validity of this model was compared to the experimental data and a satisfactory agreement was obtained. The postulated reaction mechanism was given as follows:

$$CH_4 + 2* \leftrightarrow CH_{3(*)} + H_{(*)}$$

$$CH_{3(*)} + * \leftrightarrow CH_{2(*)} + H_{(*)}$$

$$CH_{2(*)} + * \leftrightarrow CH_{(*)} + H_{(*)}$$

$$CH_{(*)} + * \leftrightarrow C_{(*)} + H_{(*)}$$

$$C_{(*)} + C_x \leftrightarrow CO + O_{(x-1)} + *$$

$$CO_2 + O_{x-1} \leftrightarrow O_x + CO$$

$$4H_{(*)} \leftrightarrow 2H_2 + 4*$$

$$H_2 + O_x \leftrightarrow O_{x-1} + H_2O$$
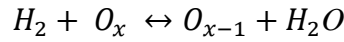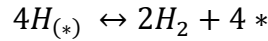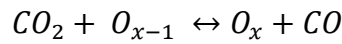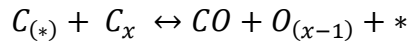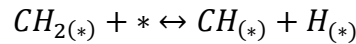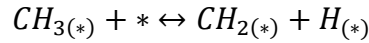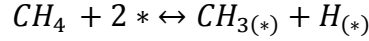
It was concluded that CH_4 dissociation functions as the RDS and the final retraction mechanism equation was defined as follows:

$$-r_A = \frac{2,1 \cdot 10^{17} \, e^{\frac{-222800}{RT}} \left(N_A - \frac{N^2_C \cdot N^2_D}{k_{Ref}} \right)}{\left(1 + 34.3 N_D^{1/2} \right)^5} \qquad (14)$$

Eq. 14 shows that r_A was based on four assumptions that included (i) CH_4 adsorption/dissociation, (ii) surface reaction of C with lattice oxygen, (iii) surface reaction of reduced site with CO_2 and (vi) surface reaction of two adsorbed hydrogen atoms. This model was concluded to be comprehensive and consistent with the experimental results and predicted whether a plug flow behavior was attained for each kinetic reaction rate in a packed bed tubular reactor.

Becerra [259] utilized the ER model as a comparison to the experimental results of DRM over Ni/Al₂O₃ catalyst reaction. The model assumed that CH_4 was non-dissociatively adsorbed on the catalyst surface in an adsorption equilibrium and that the rate-determining step is the reaction of the adsorbed species with CO_2 from the gas phase, leading directly to the products,

similar to Akpan *et al.* [258]. This ER adequately described the catalytic reactions, including the influence of the reverse water-gas shift reaction that was included as an independent side reaction. The determined kinetic parameters were found to be comparable with the ones reported in the open literature.

The Eley-Rideal type model is in a good agreement with the experimental observations although it has relatively low coverage by the published literature.

4.6.4 Langmuir Hinshelwood–Hougen Watson Model (LHHW, LH)

The LHHW models for DRM receives the literature greatest attention [42, 236] due to the conformity of the proposed mechanistic and experimental techniques. In this reaction mechanism both reactants first adsorb onto the surface (reaction 1 and 2, Figure 23) before the reaction between them takes place. Surface diffusion facilitates the interaction between adsorbed molecules and then the reaction product desorbs from the surface.
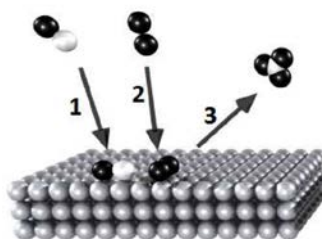
Fig. 23. Both reactants first adsorb onto the surface (reaction 1 and 2) and the product desorbs (reaction 3) from the surface [41].

The reactivity is highest when a stoichiometric amount of reactant is adsorbed on the surface and both reactants are fully dispersed over the surface. DRM catalytic reactions is alleged to follow the LH mechanism and the general reaction rate equation is [236]:

$$R_{LH} = k \frac{K_1 p_1 \; K_2 p_2}{(1 + \; K_1 p_1 \;\; + \; K_2 p_2)^2} \tag{15}$$

Gokon [42] checked the conformity of four different kinetic modeling: (i) the LH, (ii) basic power low , (iii) ER and (vi) stepwise mechanisms for DRM on Ru/γ-Al$_2$O$_3$ at temperatures of 973-1073 °K and pressure of 1 bar. It was concluded that the LH model provided the best prediction of the experimental reforming rates and was based on the assumption that both reactant species of (CH$_4$ and CO$_2$) are adsorbed onto the catalyst active sites in thermodynamic equilibrium and associatively react on the catalyst active site to form H$_2$ and CO. The reaction mechanism for the DRM was determined as:

$$R = \frac{k \, K_{CO_2} K_{CH_4} \, P_{CO_2} P_{CH_4}}{(1 + K_{CO_2} P_{CO_2} + K_{CH_4} P_{CH_4})^2} \qquad (16)$$

The adsorption equilibrium constants of the CH_4 and CO_2 are K_{CH_4} and K_{CO_2} respectively and the rate constant of the CO_2 reforming reaction is k.

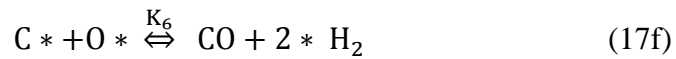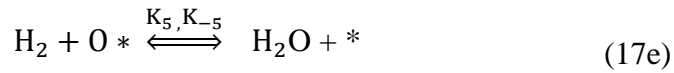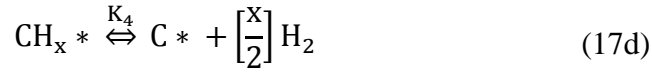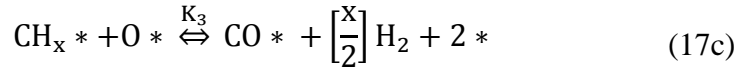Lyer *et al.* [241] described the kinetics for Co based catalyst, utilizing the LH kinetic model based on a simplified reaction mechanism involved in DRM reaction:

a. Dissociation/activation of CH_4 and CO_2.
b. Adsorption of elemental and intermediate C, H and O species on active sites.
c. Formation of product species via surface reaction.
d. Desorption of product species, *i.e.,* CO, H_2 and H_2O.

The offered mechanism incorporated carbon deposition as well as carbon removal occurred in the reaction system. On the basis of the predicted reaction mechanisms the following reaction mechanism was used [241]:

$$CO_2 + * \overset{K_1}{\Leftrightarrow} CH_x * + \left[\frac{4-x}{2}\right] H_2 \qquad (17a)$$

$$CO_2 + * \overset{K_2}{\Leftrightarrow} CO \; + \overset{K_2}{\Leftrightarrow} CO + O * \qquad (17b)$$

$$CH_x * + O * \overset{K_3}{\Leftrightarrow} CO * + \left[\frac{x}{2}\right] H_2 + 2 * \qquad (17c)$$

$$CH_x * \overset{K_4}{\Leftrightarrow} C * + \left[\frac{x}{2}\right] H_2 \qquad (17d)$$

$$H_2 + O * \overset{K_5, K_{-5}}{\Longleftrightarrow} H_2O + * \qquad (17e)$$

$$C * + O * \overset{K_6}{\Leftrightarrow} CO + 2 * H_2 \qquad (17f)$$
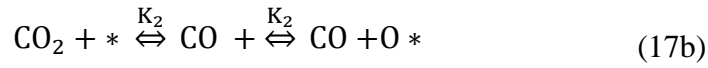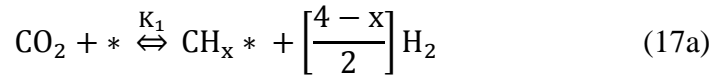
The parameter x was valued at 2 for simplicity and in order to simplify the mathematical modeling. The first and second steps (Eq. 17a and 17b) were assumed to be in equilibrium. The third step (Eq. 17c) is slow and irreversible and the fourth step (Eq. 17d) is assumed to be in equilibrium. The reaction between adsorbed oxygen and gaseous H_2 to produce water (Eq. 17e) was assumed to be reversible, but not in equilibrium (for that study). The final step (Eq. 17f) signifies the removal of accumulated carbon from the reaction system as observed in the experimental data. The expressions for the rate of formation of the products from the above reaction mechanism were written as [241]:

$$R_{CO} = \frac{K_1 K_2}{den^2} \left(\frac{P_{CH_4} \cdot P_{CO_2}}{P_{CO} \cdot P_{H_2}} \right) \left(k_3 + \frac{K_6 \cdot K_4}{P_{H_2}} \right) \tag{18a}$$

$$R_{H_2} = \frac{k_3 K_1 K_2}{den^2} \left(\frac{P_{CH_4} \cdot P_{CO_2}}{P_{CO} \cdot P_{H_2}} \right) - \frac{k_5 K_2}{den} \left(\frac{P_{H_2} \cdot P_{CO_2}}{P_{CO}} \right) + \left(\frac{K_{-5} \cdot P_{H_2O}}{den} \right) \tag{18b}$$

$$r_{H_2O} = \frac{k_5 K_2}{den} \left(\frac{P_{H_2} \cdot P_{CO_2}}{P_{CO}} \right) - \left(\frac{K_{-5} \cdot P_{H_2O}}{den} \right) \tag{18c}$$

$$den = 1 + K_1 \left(\frac{P_{CH_4}}{P_{H_2}} \right) + K_2 \left(\frac{P_{CO_2}}{P_{CO}} \right) - K_1 K_4 \left(\frac{P_{CH_4}}{P_{H_2}^2} \right) \tag{18d}$$

The parameters of the model successfully predicted the experimental data. The same study also examined a simple power-law model, which was incapable of incorporating all of the mechanistic details involved in the reaction

4.7 Summary of Kinetics and Reaction Mechanism

The DRM is a comparatively simple reaction but its mechanism appeared to be difficult to predict. There are different opinions for the nature of the intermediate reactions involved in the RDS of the process and on the methane formation scheme. The comprehensive reaction mechanisms proposed for the DRM mainly fall into two main categories. On the first one, the reactants adsorbs onto the surface followed by desorption of the reaction products. On the other one, both reactants first adsorb onto the surface and surface diffusion facilitates the interaction between adsorbed molecules, the reaction product then desorbs from the surface. It has been proposed that the rate-determining step is either the formation of the intermediate CH_xO and its interaction with hydrogen or the formation of surface carbon in CO dissociation and its hydrogenation. Ultimately, the goal of reaction kinetics exploration is greatly beneficial in optimization of catalyst design and synthesis to improve the commercialization viability of the DRM process.

5   CONCLUSION AND FUTURE DIRECTIONS

This thesis focuses on the DRM process with a comprehensive review of the catalyst design and preparation, catalytic activity and thermodynamic-kinetic analysis. Catalyst deactivation as a result of carbon deposition is the main concern of this process, which is inherently influenced by catalyst design and the chosen reaction conditions.

In comparison to the DRM, four other reforming methods are also briefly reviewed, *i.e.*, SMR, POA, ATR and Tri reforming. Currently SMR is the most often applied industrial technology and more developed than the other reforming technologies. The common feature of all reforming processes, including DRM, is the utilization of oxidizing agent to oxidize methane over heterogeneous catalysts and to produce CO and H_2 syngas in a ratio that depends both on the type of oxidant and on the thermodynamic variables. Nevertheless, all these processes suffer from the same carbon deactivation and high process costs. Interestingly, DRM is unique due to its novelty in the utilization of CO_2 as a feedstock materials instead of treating it as a waste that can potentially offset the increasing GHG emissions in the future.

Heterogeneous catalyst used in DRM normally contains active metal, support and promoter. The active metals belong to Group VIII and are divided to two groups: earth-abundant transition metals and noble metals. The majority of catalysts are based on Ni due to its high activity and acceptable market price. The noble metals, Rh, Ru, Ir, Pt and Pd have a promising catalytic performance and low sensitivities to carbon deposits. It is shown that among the active metals, Ru performs best in terms of stability and activity. However, the high cost of noble metals still challenges their implementation in industrial scales and thus motivates researchers to examine their incorporation as second metal in low percentage as bimetallic catalyst based on Ni or Co. Importantly, combining active metals such as Ni, Co or noble metals to create bimetallic alloy can produce catalysts with optimized activity and stability, while at a reasonable cost.

It is accepted that the catalyst support plays an important role as catalyst carrier and its contribution to the catalysis activity and coke deposition prevention is considerable. A significant factor effecting carbon deposition is the catalyst surface basicity. In particular, it has been demonstrated that carbon formation can be dramatically reduced when the active metal is supported on a metal oxide carrier with Lewis basicity. Proper selection of the support can significantly modify the catalytic properties of a given metal at DRM conditions and change the tendency towards sintering prevention and resistance to carbon deposition. It is concluded that the Al_2O_3 and TiO_2 supports in many cases contribute to enhanced catalytic activity and coke deposition inhibition.

The catalyst promoters are non-active substances that are proposed to improve the catalytic performance through surface structural effects. Promoters enhance the active metal dispersion over the support, benefitting from the existence of strong metal–support interactions that change the basicity of the catalysts towards more basic state. Among the known studies today, the two types of promoters that show remarkable high activity and stability, *i.e.,* Ce and

ZrO_2 promoters. Both show enhancement of CO_2 dissociation to form oxygen intermediates that can gasify the coke deposits over Ni supported onto Al_2O_3.

In this work, special attention is also paid to the investigation of catalysts design and synthesis. Despite the fact that the catalyst preparation methodology is already well defined, the realization to obtain the exact structure, morphology and function of the produced catalyst is still hard to achieve and drives the further investigation on more controllable preparation and characterization methods.

DRM thermodynamic equilibrium analysis uses the ΔG minimization methods to predict reactions mechanism and is interconnected to the kinetic reaction mechanisms. Thermodynamic analysis shows that the reaction temperature, pressure, and reactants (CO_2/CH_4) ratio significantly influence the reactants equilibrium, products composition and carbon formation. In general, the DRM is favored with low pressures close to 1 bar, temperature range of 770-1170 °K and reactant ratio close to unity while carbon deposition inhibition is considered as the main challenges for the research in this field.

The DRM is a comparatively simple reaction but its mechanism appeared to be difficult to predict. There are different opinions for the nature of the intermediate reactions involved in the RDS of the process and on the methane formation scheme. The comprehensive reaction mechanisms proposed for the DRM mainly fall into two main categories. On the first one, the reactants adsorb onto the surface followed by desorption of the reaction products. On the other one, both reactants first adsorb onto the surface and surface diffusion facilitates the interaction between the adsorbed molecules. The reaction product then desorbs from the surface. It has been proposed that the RDS is either the formation of the intermediate CH_xO and its interaction with hydrogen or the formation of surface carbon in CO dissociation and its hydrogenation. Ultimately, the goal of reaction kinetics exploration is greatly beneficial in optimization of catalyst design and synthesis to improve the commercial viability of the DRM process.

The DRM process has a promising future in technological developments. The growing interest in natural gas or shale gas exploitation around the world together with the growing amounts of captured CO_2 as regulated by the developed countries, the DRM research can be the perfect solution with the superior advantage of utilizing CO_2 as oxidizing agent for syngas manufacturing. The challenges of the DRM process involve the development of novel research aiming to optimize this catalytic process. Researchers should focus on new catalytic materials development that are more resistant to deactivation and on the development of better operating conditions aiming to reduce the DRM process cost.

6   REFERENCES

1.   Bayer, P., et al., *Greenhouse gas emission savings of ground source heat pump systems in Europe: A review.* Renewable and Sustainable Energy Reviews, 2012. **16**(2): p. 1256-1267.

2.   da Graça Carvalho, M., *EU energy and climate change strategy.* Energy, 2012. **40**(1): p. 19-22.

3.   Shackley, S., et al., *The acceptability of CO2 capture and storage (CCS) in Europe: An assessment of the key determining factors: Part 2. The social acceptability of CCS and the wider impacts and repercussions of its implementation.* International Journal of Greenhouse Gas Control, 2009. **3**(3): p. 344-356.

4.   A. Hanif, T.S.P., and MLH Green/Univ. of Oxford, *<possible utilisation of CO2 on NG field using DRM to Syngas.pdf>.* SPE Asia Pacific Oil and Gas Conference 2002, 2002.

5.   Dunk, D.R., *assesmnet of subsea acosystem impact* 2009, international energy agency, IEA inviromental projects UK.

6.   *<Application of Geoscience Technology in a Geologic Study of the Natuna Gas Field, Natuna Sea, Offshore Indonesia.pdf>.*

7.   Peter Styring (The University of Sheffield), D.J.E., *Carbon Capture and Utilisation in the green economy*. 2011: The University of Sheffield.

8.   Sudiro, M. and A. Bertucco, *Synthetic Fuels by a Limited CO2 Emission Process Which Uses Both Fossil and Solar Energy.* Energy & Fuels, 2007. **21**(6): p. 3668-3675.

9.   Akande, A., et al., *Kinetic modeling of hydrogen production by the catalytic reforming of crude ethanol over a co-precipitated catalyst in a packed bed tubular reactor.* International Journal of Hydrogen Energy, 2006. **31**(12): p. 1707-1715.

10.   Antonio C. D. Freitas, R.G., *<Thermodynamic analysis of methane reforming with CO2, CO2+H2O and CO2+O2 for hydrogen and synthesis gas production.pdf>.* 2006

11.   Ahmadpour, J. and M. Taghizadeh, *Catalytic conversion of methanol to propylene over high-silica mesoporous ZSM-5 zeolites prepared by different combinations of mesogenous templates.* Journal of Natural Gas Science and Engineering, 2015. **23**(0): p. 184-194.

12.   Al-Sobhi, S.A. and A. Elkamel, *Simulation and optimization of natural gas processing and production network consisting of LNG, GTL, and methanol facilities.* Journal of Natural Gas Science and Engineering, 2015. **23**(0): p. 500-508.

13.   Hu, Y.H., *Advances in Catalysts for CO2Reforming of Methane.* 2010. **1056**: p. 155-174.

14.   Ghorbani, A., M. Jafari, and M.R. Rahimpour, *A comparative simulation of a novel gas to liquid (GTL) conversion loop as an alternative to a certain refinery gas flare.* Journal of Natural Gas Science and Engineering, 2013. **11**(0): p. 23-38.

15.   Johnsen, K., et al., *Sorption-enhanced steam reforming of methane in a fluidized bed reactor with dolomite as -acceptor.* Chemical Engineering Science, 2006. **61**(4): p. 1195-1202.

16. Li, Y., et al., *Thermodynamic analysis of autothermal steam and CO2 reforming of methane.* International Journal of Hydrogen Energy, 2008. **33**(10): p. 2507-2514.

17. Barelli, L., et al., *Hydrogen production through sorption-enhanced steam methane reforming and membrane technology: A review.* Energy, 2008. **33**(4): p. 554-570.

18. Ruiz-Trejo, E., et al., *Partial oxidation of methane using silver/gadolinia-doped ceria composite membranes.* Chemical Engineering Science, 2015. **127**: p. 269-275.

19. Trimm, D.L., *Catalysts for the control of coking during steam reforming.* Catalysis Today, 1999. **49**(1–3): p. 3-10.

20. Li, S., et al., *Steam reforming of ethanol over Ni/ZrO2 catalysts: Effect of support on product distribution.* International Journal of Hydrogen Energy, 2012. **37**(3): p. 2940-2949.

21. Horiuchi, T., et al., *Suppression of carbon deposition in the CO2-reforming of CH4 by adding basic metal oxides to a Ni/Al2O3 catalyst.* Applied Catalysis A: General, 1996. **144**(1–2): p. 111-120.

22. Nguyen, T.H., et al., *Partial oxidation of methane over Ni0/La2O3 bifunctional catalyst II: Global kinetics of methane total oxidation, dry reforming and partial oxidation.* Applied Catalysis B: Environmental, 2015. **165**(0): p. 389-398.

23. Roussière, T.L., *<2013_Roussiere_CatRefMethaneinPresenceofCO2andH2OatHighPress_Dr_rernat_KIT_final.pdf>*, in *Fakultät für Chemie und Biowissenschaften*. 2003, Karlsruher Institut für Technologie (KIT) - Universitätsbereich.

24. Chen, W.-H., *CO2 conversion for syngas production in methane catalytic partial oxidation.* Journal of CO2 Utilization, 2014. **5**(0): p. 1-9.

25. Andrew P.E. York, T.X., and Malcolm L.H. Green, *<Brief overview of the partial oxidation of methane to synthesis gas.pdf>.* 2003.

26. Wang, Y., et al., *Effect of Pr addition on the properties of Ni/Al2O3 catalysts with an application in the autothermal reforming of methane.* International Journal of Hydrogen Energy, 2014. **39**(2): p. 778-787.

27. Zahedi nezhad, M., S. Rowshanzamir, and M.H. Eikani, *Autothermal reforming of methane to synthesis gas: Modeling and simulation.* International Journal of Hydrogen Energy, 2009. **34**(3): p. 1292-1300.

28. Gao, J., et al., *Methane autothermal reforming with CO2 and O2 to synthesis gas at the boundary between Ni and ZrO2.* International Journal of Hydrogen Energy, 2009. **34**(9): p. 3734-3742.

29. Hou, Z., et al., *Deactivation of Ni catalysts during methane autothermal reforming with CO2 and O2 in a fluidized-bed reactor.* Journal of Catalysis, 2007. **250**(2): p. 331-341.

30. Snoeck, J.W., G.F. Froment, and M. Fowles, *Steam/CO2 Reforming of Methane. Carbon Filament Formation by the Boudouard Reaction and Gasification by CO2, by H2, and by Steam: Kinetic Study.* Industrial & Engineering Chemistry Research, 2002. **41**(17): p. 4252-4265.

31. *<Carbon dioxide reforming of methane with Pt catalysts using.pdf>.*

32. Kim, D.H., et al., *The catalytic stability of TiO2-shell/Ni-core catalysts for CO2 reforming of CH4.* Applied Catalysis A: General, 2015. **495**: p. 184-191.

33. Ahmed, S.A.A.-F., *Effects of promoters on methane dry reforming over Ni catalyst on a mixed (a-Al2O3+TiO2-P25) support.* International Journal of the Physical Sciences, 2011. **6**(36).

34. Li, Z., Y. Kathiraser, and S. Kawi, *Facile Synthesis of High Surface Area Yolk-Shell Ni@Ni Embedded SiO2via Ni Phyllosilicate with Enhanced Performance for CO2Reforming of CH4.* ChemCatChem, 2015. **7**(1): p. 160-168.

35. Hu, Y.H. and E. Ruckenstein, *An optimum NiO content in the CO2 reforming of CH4 with NiO/MgO solid solution catalysts.* Catalysis Letters, 1996. **36**(3-4): p. 145-149.

36. Fan, M.-S., A.Z. Abdullah, and S. Bhatia, *Catalytic Technology for Carbon Dioxide Reforming of Methane to Synthesis Gas.* ChemCatChem, 2009. **1**(2): p. 192-208.

37. *<Carbon Dioxide Reforming of Methane To Produce synthesis gas over metal supported catalysts.pdf>.*

38. Rostrupnielsen, J.R. and J.H.B. Hansen, *CO2-Reforming of Methane over Transition Metals.* Journal of Catalysis, 1993. **144**(1): p. 38-49.

39. Nagaoka, K., et al., *Carbon Deposition during Carbon Dioxide Reforming of Methane—Comparison between Pt/Al2O3 and Pt/ZrO2.* Journal of Catalysis, 2001. **197**(1): p. 34-42.

40. Chunyang Ji, L.G., Jiawei Zhang, Keying Shi, *<A Study on the Kinetics of the Catalytic Reforming Reaction of CH4 with CO2 Determination of the Reaction Order.pdf>.* 2003

41. Herbschleb, C.T., *<Imaging Catalysts under Realistic Conditions.pdf>*, in *Faculty of Science, Leiden University*. 2011: Faculty of Science, Leiden University.

42. Gokon, N., et al., *Kinetics of CO2 reforming of methane by catalytically activated metallic foam absorber for solar receiver-reactors.* International Journal of Hydrogen Energy, 2009. **34**(4): p. 1787-1800.

43. Takezawa, N. and N. Iwasa, *Steam reforming and dehydrogenation of methanol: Difference in the catalytic functions of copper and group VIII metals.* Catalysis Today, 1997. **36**(1): p. 45-56.

44. Liu, D., et al., *Methane reforming with carbon dioxide over a Ni/ZiO2–SiO2 catalyst: Influence of pretreatment gas atmospheres.* International Journal of Hydrogen Energy, 2012. **37**(13): p. 10135-10144.

45.   Sajjadi, S.M., M. Haghighi, and F. Rahmani, *Sol–gel synthesis of Ni–Co/Al2O3–MgO–ZrO2 nanocatalyst used in hydrogen production via reforming of CH4/CO2 greenhouse gases.* Journal of Natural Gas Science and Engineering, 2015. **22**: p. 9-21.

46.   Djaidja, A., et al., *Study of Ni–M/MgO and Ni–M–Mg/Al (M=Fe or Cu) catalysts in the CH4–CO2 and CH4–H2O reforming.* International Journal of Hydrogen Energy, 2015. **40**(14): p. 4989-4995.

47.   Yahyavi, S.R., et al., *Ultrasound-assisted synthesis and physicochemical characterization of Ni–Co/Al2O3–MgO nanocatalysts enhanced by different amounts of MgO used for CH4/CO2 reforming.* Energy Conversion and Management, 2015. **97**: p. 273-281.

48.   Song, C. and W. Pan, *Tri-reforming of methane: a novel concept for catalytic production of industrially useful synthesis gas with desired H2/CO ratios.* Catalysis Today, 2004. **98**(4): p. 463-484.

49.   D.Wolf∗, O.V.B., M. Baerns, *<An evolutionary approach in the combinatorial selection and optimization of catalytic materials.pdf>.* 2000.

50.   Shishido, T., et al., *Active Cu/ZnO and Cu/ZnO/Al2O3 catalysts prepared by homogeneous precipitation method in steam reforming of methanol.* Applied Catalysis A: General, 2004. **263**(2): p. 249-253.

51.   Widegren, J.A. and R.G. Finke, *A review of the problem of distinguishing true homogeneous catalysis from soluble or other metal-particle heterogeneous catalysis under reducing conditions.* Journal of Molecular Catalysis A: Chemical, 2003. **198**(1–2): p. 317-341.

52.   Eriksson, S., et al., *Preparation of catalysts from microemulsions and their applications in heterogeneous catalysis.* Applied Catalysis A: General, 2004. **265**(2): p. 207-219.

53.   Sahli, N., et al., *Ni catalysts from NiAl2O4 spinel for CO2 reforming of methane.* Catalysis Today, 2006. **113**(3–4): p. 187-193.

54.   Ashcroft, A.T., et al., *Partial oxidation of methane to synthesis gas using carbon dioxide.* Nature, 1991. **352**(6332): p. 225-226.

55.   Chen, D., et al., *Deactivation during carbon dioxide reforming of methane over Ni catalyst: microkinetic analysis.* Chemical Engineering Science, 2001. **56**(4): p. 1371-1379.

56.   de Sousa, F.F., et al., *Nanostructured Ni-containing spinel oxides for the dry reforming of methane: Effect of the presence of cobalt and nickel on the deactivation behaviour of catalysts.* International Journal of Hydrogen Energy, 2012. **37**(4): p. 3201-3212.

57.   Ruckenstein, E. and Y.H. Hu, *Carbon dioxide reforming of methane over nickel/alkaline earth metal oxide catalysts.* Applied Catalysis A: General, 1995. **133**(1): p. 149-161.

58.   Fidalgo, B. and J.Á. MenÉNdez, *Carbon Materials as Catalysts for Decomposition and CO2 Reforming of Methane: A Review.* Chinese Journal of Catalysis, 2011. **32**(1-2): p. 207-216.

59.   Zhang, Z. and X.E. Verykios, *Carbon dioxide reforming of methane to synthesis gas over Ni/La2O3 catalysts.* Applied Catalysis A: General, 1996. **138**(1): p. 109-133.

60.   Amin, M.H., et al., *Understanding the role of lanthanide promoters on the structure–activity of nanosized Ni/γ-Al2O3 catalysts in carbon dioxide reforming of methane.* Applied Catalysis A: General, 2015. **492**: p. 160-168.

61.   Yu, M.J., et al., *The promoting role of Ag in Ni-CeO2 catalyzed CH4-CO2 dry reforming reaction.* Applied Catalysis B-Environmental, 2015. **165**(0): p. 43-56.

62.   Ilenia Rossetti a, N.P., Lucio Forni a,∗, *<Promoters effect in Ru C ammonia synthesis catalyst.pdf>.* 2000.

63.   Yejun Qiu, J.C., , Jiyan Zhang, *<Effect of CeO2 and CaO Promoters on Ignition Performance for Partial Oxidation of Methane over Ni MgO Al2O3 Catalyst.pdf>.* 2008.

64.   Yejun Qiu, J.C., Jiyan Zhang, *<Effects of CeO2 and CaO composite promoters on the properties of eggshell Ni MgO-Al2O3 catalysts for partial oxidation of methane to synga.pdf>.* 2009.

65.   Qin, H., et al., *Effect of La2O3 promoter on NiO/Al2O3 catalyst in CO methanation.* Korean Journal of Chemical Engineering, 2014. **31**(7): p. 1168-1173.

66.   Zhang, G., et al., *Catalytic performance of activated carbon supported cobalt catalyst for CO2 reforming of CH4.* J Colloid Interface Sci, 2014. **433**: p. 149-55.

67.   Zhang, Z.L., et al., *Reforming of Methane with Carbon Dioxide to Synthesis Gas over Supported Rhodium Catalysts: I. Effects of Support and Metal Crystallite Size on Reaction Activity and Deactivation Characteristics.* Journal of Catalysis, 1996. **158**(1): p. 51-63.

68.   Ruckenstein, E. and Y. Hang Hu, *Role of Support in CO2Reforming of CH4to Syngas over Ni Catalysts.* Journal of Catalysis, 1996. **162**(2): p. 230-238.

69.   Jüntgen, H., *Activated carbon as catalyst support: A review of new research results.* Fuel, 1986. **65**(10): p. 1436-1446.

70.   Aksoylu, A.E., et al., *The effects of different activated carbon supports and support modifications on the properties of Pt/AC catalysts.* Carbon, 2001. **39**(2): p. 175-185.

71.   Kawi, S. and Y. Kathiraser, *CO2 as an Oxidant for High Temperature Reactions.* Frontiers in Energy Research, 2015. **3**.

72.   A. Maeda, F.Y., K. Kunimori, T. Uchijima, *<Effect of strong metal-support interaction (SMSI) on ethylene hydroformylation over niobia-supported palladium catalysts.pdf>.* 1989

73.   Huang, T., et al., *Methane reforming reaction with carbon dioxide over SBA-15 supported Ni–Mo bimetallic catalysts.* Fuel Processing Technology, 2011. **92**(10): p. 1868-1875.

74.   Michael C.J. Bradford1 , M.A.V., *<The role of metal–support interactions in CO2 reforming of CH4.pdf>.* 1999

75.   Chen, Y.-G., et al., *Catalytic Performance and Catalyst Structure of Nickel–Magnesia Catalysts for CO2 Reforming of Methane.* Journal of Catalysis, 1999. **184**(2): p. 479-490.

76.   Cheng, Z.X., et al., *Role of support in CO2 reforming of CH4 over a Ni/γ-Al2O3 catalyst.* Applied Catalysis A: General, 2001. **205**(1-2): p. 31-36.

77.   Zhang, J., H. Wang, and A.K. Dalai, *Development of stable bimetallic catalysts for carbon dioxide reforming of methane.* Journal of Catalysis, 2007. **249**(2): p. 300-310.

78.   Guo, J., et al., *Dry reforming of methane over nickel catalysts supported on magnesium aluminate spinels.* Applied Catalysis A: General, 2004. **273**(1–2): p. 75-82.

79.   Liu, D., et al., *MCM-41 supported nickel-based bimetallic catalysts with superior stability during carbon dioxide reforming of methane: Effect of strong metal–support interaction.* Journal of Catalysis, 2009. **266**(2): p. 380-390.

80.   Ferreira-Aparicio, P., A. Guerrero-Ruiz, and I. Rodríguez-Ramos, *Comparative study at low and medium reaction temperatures of syngas production by methane reforming with carbon dioxide over silica and alumina supported catalysts.* Applied Catalysis A: General, 1998. **170**(1): p. 177-187.

81.   Goula, M.A., A.A. Lemonidou, and A.M. Efstathiou, *Characterization of Carbonaceous Species Formed during Reforming of CH4with CO2over Ni/CaO–Al2O3Catalysts Studied by Various Transient Techniques.* Journal of Catalysis, 1996. **161**(2): p. 626-640.

82.   Benguerba, Y., et al., *Numerical investigation of the optimal operative conditions for the dry reforming reaction in a fixed-bed reactor: role of the carbon deposition and gasification reactions.* Reaction Kinetics, Mechanisms and Catalysis, 2015: p. 1-15.

83.   Inui, T., *Rapid catalytic reforming of methane with CO2 and its application to other reactions.* Applied Organometallic Chemistry, 2001. **15**(2): p. 87-94.

84.   Pakhare, D. and J. Spivey, *A review of dry (CO2) reforming of methane over noble metal catalysts.* Chemical Society Reviews, 2014. **43**(22): p. 7813-7837.

85.   Keiichi Tomishige, Y.-g.C., and Kaoru Fujimoto, *<Studies on Carbon Deposition in CO2Reforming of CH4over Nickel–Magnesia Solid Solution Catalysts.pdf>.* 1998.

86.   Lee, S.-H., et al., *Tri-reforming of CH4 using CO2 for production of synthesis gas to dimethyl ether.* Catalysis Today, 2003. **87**(1–4): p. 133-137.

87.   Kroll, V.C.H., H.M. Swaan, and C. Mirodatos, *Methane Reforming Reaction with Carbon Dioxide Over Ni/SiO2Catalyst: I. Deactivation Studies.* Journal of Catalysis, 1996. **161**(1): p. 409-422.

88.   Slagtern, A., et al., *Specific Features Concerning the Mechanism of Methane Reforming by Carbon Dioxide over Ni/La2O3Catalyst.* Journal of Catalysis, 1997. **172**(1): p. 118-126.

89.   Kim, J.-H., et al., *Effect of metal particle size on coking during CO2 reforming of CH4 over Ni–alumina aerogel catalysts.* Applied Catalysis A: General, 2000. **197**(2): p. 191-200.

90.   Shishido, T., et al., *CO2 reforming of CH4 over Ni/Mg–Al oxide catalysts prepared by solid phase crystallization method from Mg–Al hydrotalcite-like precursors.* Catalysis Letters, 2001. **73**(1): p. 21-26.

91.   Lovell, E.C., J. Scott, and R. Amal, *Ni-SiO(2) catalysts for the carbon dioxide reforming of methane: varying support properties by flame spray pyrolysis.* Molecules, 2015. **20**(3): p. 4594-609.

92.   Cai, W., et al., *Highly Dispersed Nickel-Containing Mesoporous Silica with Superior Stability in Carbon Dioxide Reforming of Methane: The Effect of Anchoring.* Materials, 2014. **7**(3): p. 2340-2355.

93.   Jung, O.-S.J.a.K.-D., *<CH4 Dry Reforming on Alumina-Supported Nickel Catalyst.pdf>.* 2002.

94.   Bradford, M.C.J. and M.A. Vannice, *CO2Reforming of CH4.* Catalysis Reviews, 1999. **41**(1): p. 1-42.

95.   Fidalgo, B., et al., *Synthesis of carbon-supported nickel catalysts for the dry reforming of CH4.* Fuel Processing Technology, 2010. **91**(7): p. 765-769.

96.   Helveg, S., J. Sehested, and J.R. Rostrup-Nielsen, *Whisker carbon in perspective.* Catalysis Today, 2011. **178**(1): p. 42-46.

97.   Ma, J., et al., *A short review of catalysis for CO2 conversion.* Catalysis Today, 2009. **148**(3-4): p. 221-231.

98.   Nikoo, M.K. and N.A.S. Amin, *Thermodynamic analysis of carbon dioxide reforming of methane in view of solid carbon formation.* Fuel Processing Technology, 2011. **92**(3): p. 678-691.

99.   Takanabe, K., et al., *Titania-supported cobalt and nickel bimetallic catalysts for carbon dioxide reforming of methane.* Journal of Catalysis, 2005. **232**(2): p. 268-275.

100.   Rostrup-Nielsen, J.R., *Syngas in perspective.* Catalysis Today, 2002. **71**(3–4): p. 243-247.

101.   Djinović, P., et al., *Catalytic syngas production from greenhouse gasses: Performance comparison of Ru-Al2O3 and Rh-CeO2 catalysts.* Chemical Engineering and Processing: Process Intensification, 2011. **50**(10): p. 1054-1062.

102.   Yoshida, K., et al., *Oxidative steam reforming of methane over Ni/α-Al2O3 modified with trace noble metals.* Applied Catalysis A: General, 2009. **358**(2): p. 186-192.

103.   Erdohelyi, A., J. Cserenyi, and F. Solymosi, *Activation of CH4 and Its Reaction with CO2 over Supported Rh Catalysts.* Journal of Catalysis, 1993. **141**(1): p. 287-299.

104. Souza, G.d., N.R. Marcilio, and O.W. Perez-Lopez, *Dry reforming of methane at moderate temperatures over modified Co-Al Co-precipitated catalysts.* Materials Research, 2014. **17**(4): p. 1047-1055.

105. Bradford, M.C.J. and M.A. Vannice, *Catalytic reforming of methane with carbon dioxide over nickel catalysts I. Catalyst characterization and activity.* Applied Catalysis A: General, 1996. **142**(1): p. 73-96.

106. Basini, L. and D. Sanfilippo, *Molecular Aspects in Syn-Gas Production: The CO2-Reforming Reaction Case.* Journal of Catalysis, 1995. **157**(1): p. 162-178.

107. Bitter, J.H., K. Seshan, and J.A. Lercher, *The State of Zirconia Supported Platinum Catalysts for CO2/CH4Reforming.* Journal of Catalysis, 1997. **171**(1): p. 279-286.

108. Ferreira-Aparicio, P., et al., *Mechanistic aspects of the dry reforming of methane over ruthenium catalysts.* Applied Catalysis A: General, 2000. **202**(2): p. 183-196.

109. Nagaoka, K., M. Okamura, and K.-i. Aika, *Titania supported ruthenium as a coking-resistant catalyst for high pressure dry reforming of methane.* Catalysis Communications, 2001. **2**(8): p. 255-260.

110. Ferreira-Aparicio, P., et al., *A Transient Kinetic Study of the Carbon Dioxide Reforming of Methane over Supported Ru Catalysts.* Journal of Catalysis, 1999. **184**(1): p. 202-212.

111. Hou, Z., *Production of synthesis gas via methane reforming with CO2 on noble metals and small amount of noble-(Rh-) promoted Ni catalysts.* 2006

112. Ghelamallah, M. and P. Granger, *Supported-induced effect on the catalytic properties of Rh and Pt-Rh particles deposited on La2O3 and mixed α-Al2O3-La2O3 in the dry reforming of methane.* Applied Catalysis A: General, 2014. **485**(0): p. 172-180.

113. Arandiyan, H., et al., *Effects of noble metals doped on mesoporous LaAlNi mixed oxide catalyst and identification of carbon deposit for reforming CH4 with CO2.* Journal of Chemical Technology and Biotechnology, 2014. **89**(3): p. 372-381.

114. Nematollahi, B., M. Rezaei, and M. Khajenoori, *Combined dry reforming and partial oxidation of methane to synthesis gas on noble metal catalysts.* International Journal of Hydrogen Energy, 2011. **36**(4): p. 2969-2978.

115. Hou, Z., et al., *Production of synthesis gas via methane reforming with CO on noble metals and small amount of noble-(Rh-) promoted Ni catalysts.* International Journal of Hydrogen Energy, 2006. **31**(5): p. 555-561.

116. Matsui, N.-o., et al., *Reaction mechanisms of carbon dioxide reforming of methane with Ru-loaded lanthanum oxide catalyst.* Applied Catalysis A: General, 1999. **179**(1–2): p. 247-256.

117. Usman, M., W.M.A. Wan Daud, and H.F. Abbas, *Dry reforming of methane: Influence of process parameters—A review.* Renewable and Sustainable Energy Reviews, 2015. **45**(0): p. 710-744.

118.   Tsyganok, A.I., et al., *Dry reforming of methane over supported noble metals: a novel approach to preparing catalysts.* Catalysis Communications, 2003. **4**(9): p. 493-498.

119.   Al-Fatesh, A., *Suppression of carbon formation in CH4–CO2 reforming by addition of Sr into bimetallic Ni–Co/γ-Al2O3 catalyst.* Journal of King Saud University - Engineering Sciences, 2015. **27**(1): p. 101-107.

120.   Choudhary, V.R. and A.S. Mamman, *Simultaneous oxidative conversion and CO2 or steam reforming of methane to syngas over CoO–NiO–MgO catalyst.* Journal of Chemical Technology & Biotechnology, 1998. **73**(4): p. 345-350.

121.   Li, X., et al., *Ni-Co bimetallic catalyst for CH4 reforming with CO2.* Frontiers of Chemical Engineering in China, 2010. **4**(4): p. 476-480.

122.   Koh, A.C.W., et al., *Hydrogen or synthesis gas production via the partial oxidation of methane over supported nickel–cobalt catalysts.* International Journal of Hydrogen Energy, 2007. **32**(6): p. 725-730.

123.   Zhang, J., H. Wang, and A.K. Dalai, *Effects of metal content on activity and stability of Ni-Co bimetallic catalysts for CO2 reforming of CH4.* Applied Catalysis A: General, 2008. **339**(2): p. 121-129.

124.   Fan, M.-S., A.Z. Abdullah, and S. Bhatia, *Utilization of greenhouse gases through carbon dioxide reforming of methane over Ni–Co/MgO–ZrO2: Preparation, characterization and activity studies.* Applied Catalysis B: Environmental, 2010. **100**(1–2): p. 365-377.

125.   Lu*, S.W.a.G.Q.M., *<Carbon Dioxide Reforming of Methane To Produce Synthesis Gas over Metal Supported Catalysts State of the Art.pdf>.* 1995.

126.   de Lima, S. and J. Assaf, *Ni–Fe Catalysts Based on Perovskite-type Oxides for Dry Reforming of Methane to Syngas.* Catalysis Letters, 2006. **108**(1-2): p. 63-70.

127.   Nam, J.W., et al., *Methane Dry Reforming over Well-dispersed Ni Catalyst Prepared from Perovskite-type Mixed Oxides*, in *Studies in Surface Science and Catalysis*, D.S.F.F.A.V. A. Parmaliana and F. Arena, Editors. 1998, Elsevier. p. 843-848.

128.   Kim, J., et al., *Carbon dioxide reforming of methane to synthesis gas over LaNi1−x Cr x O3 perovskite catalysts.* Korean Journal of Chemical Engineering, 2012. **29**(10): p. 1329-1335.

129.   Kapokova, L., et al., *Dry reforming of methane over LnFe 0.7Ni 0.3O 3− δ perovskites: Influence of Ln nature.* Catalysis Today, 2011. **164**(1): p. 227-233.

130.   Cheng, H., et al., *Effects of noble metal-doping on Ni/La2O3–ZrO2 catalysts for dry reforming of coke oven gas.* International Journal of Hydrogen Energy, 2014. **39**(24): p. 12604-12612.

131.   Li, D., Y. Nakagawa, and K. Tomishige, *Methane reforming to synthesis gas over Ni catalysts modified with noble metals.* Applied Catalysis A: General, 2011. **408**(1–2): p. 1-24.

132.   García-Diéguez, M., et al., *Characterization of alumina-supported Pt, Ni and PtNi alloy catalysts for the dry reforming of methane.* Journal of Catalysis, 2010. **274**(1): p. 11-20.

133.   Tomishige, K., et al., *Catalyst Design of Pt-Modified Ni/Al2O3 Catalyst with Flat Temperature Profile in Methane Reforming with CO2 and O2.* Catalysis Letters, 2002. **84**(1-2): p. 69-74.

134.   Tsubaki, N., S. Sun, and K. Fujimoto, *Different Functions of the Noble Metals Added to Cobalt Catalysts for Fischer–Tropsch Synthesis.* Journal of Catalysis, 2001. **199**(2): p. 236-246.

135.   Dias, J.A.C. and J.M. Assaf, *Autothermal reforming of methane over Ni/γ-Al2O3 catalysts: the enhancement effect of small quantities of noble metals.* Journal of Power Sources, 2004. **130**(1–2): p. 106-110.

136.   Hao, Z., et al., *Characterization of aerogel Ni/Al2O3 catalysts and investigation on their stability for CH4-CO2 reforming in a fluidized bed.* Fuel Processing Technology, 2009. **90**(1): p. 113-121.

137.   Hao, Z., et al., *Fluidization characteristics of aerogel Co/Al2O3 catalyst in a magnetic fluidized bed and its application to CH4–CO2 reforming.* Powder Technology, 2008. **183**(1): p. 46-52.

138.   Barroso-Quiroga, M.M. and A.E. Castro-Luna, *Catalytic activity and effect of modifiers on Ni-based catalysts for the dry reforming of methane.* International Journal of Hydrogen Energy, 2010. **35**(11): p. 6052-6056.

139.   Chang, J.-S., et al., *Thermogravimetric analyses and catalytic behaviors of zirconia-supported nickel catalysts for carbon dioxide reforming of methane.* Catalysis Today, 2006. **115**(1–4): p. 186-190.

140.   Özkara-Aydınoğlu, Ş., E. Özensoy, and A.E. Aksoylu, *The effect of impregnation strategy on methane dry reforming activity of Ce promoted Pt/ZrO2.* International Journal of Hydrogen Energy, 2009. **34**(24): p. 9711-9722.

141.   Wang, H.Y. and E. Ruckenstein, *Carbon dioxide reforming of methane to synthesis gas over supported rhodium catalysts: the effect of support.* Applied Catalysis A: General, 2000. **204**(1): p. 143-152.

142.   Ballarini, A.D., et al., *Reforming of CH4 with CO2 on Pt-supported catalysts: Effect of the support on the catalytic behaviour.* Catalysis Today, 2005. **107–108**(0): p. 481-486.

143.   Wang, H.Y. and E. Ruckenstein, *CO2 reforming of CH4 over Co/MgO solid solution catalysts — effect of calcination temperature and Co loading.* Applied Catalysis A: General, 2001. **209**(1–2): p. 207-215.

144.   Jing, Q.S., et al., *Effective reforming of methane with CO2 and O2 to low H2/CO ratio syngas over Ni/MgO–SiO2 using fluidized bed reactor.* Energy Conversion and Management, 2004. **45**(20): p. 3127-3137.

145.   Pietraszek, A., et al., *The influence of the support modification over Ni-based catalysts for dry reforming of methane reaction.* Catalysis Today, 2011. **176**(1): p. 267-271.

146.   Jang, W.-J., et al., *H2 and CO production over a stable Ni–MgO–Ce0.8Zr0.2O2 catalyst from CO2 reforming of CH4.* International Journal of Hydrogen Energy, 2013. **38**(11): p. 4508-4512.

147. Safariamin, M., et al., *Dry reforming of methane in the presence of ruthenium-based catalysts.* Comptes Rendus Chimie, 2009. **12**(6–7): p. 748-753.

148. Liu, D., et al., *Carbon dioxide reforming of methane to synthesis gas over Ni-MCM-41 catalysts.* Applied Catalysis A: General, 2009. **358**(2): p. 110-118.

149. Arbag, H., et al., *Activity and stability enhancement of Ni-MCM-41 catalysts by Rh incorporation for hydrogen from dry reforming of methane.* International Journal of Hydrogen Energy, 2010. **35**(6): p. 2296-2304.

150. Zhang, M., et al., *Structural Characterization of Highly Stable Ni/SBA-15 Catalyst and Its Catalytic Performance for Methane Reforming with CO2.* Chinese Journal of Catalysis, 2006. **27**(9): p. 777-781.

151. Huang, J., et al., *Carbon dioxide reforming of methane over Ni/Mo/SBA-15-La2O3 catalyst: Its characterization and catalytic performance.* Journal of Natural Gas Chemistry, 2011. **20**(5): p. 465-470.

152. Effendi, A., et al., *Characterisation of carbon deposits on Ni/SiO2 in the reforming of CH4–CO2 using fixed- and fluidised-bed reactors.* Catalysis Communications, 2003. **4**(4): p. 203-207.

153. Zhu, J., et al., *Synthesis gas production from CO2 reforming of methane over Ni–Ce/SiO2 catalyst: The effect of calcination ambience.* International Journal of Hydrogen Energy, 2013. **38**(1): p. 117-126.

154. Sutthiumporn, K., et al., *CO2 dry-reforming of methane over La0.8Sr0.2Ni0.8M0.2O3 perovskite (M = Bi, Co, Cr, Cu, Fe): Roles of lattice oxygen on C–H activation and carbon suppression.* International Journal of Hydrogen Energy, 2012. **37**(15): p. 11195-11207.

155. Soria, M.A., et al., *Thermodynamic and experimental study of combined dry and steam reforming of methane on Ru/ ZrO2-La2O3 catalyst at low temperature.* International Journal of Hydrogen Energy, 2011. **36**(23): p. 15212-15220.

156. Amin, M.H.T., James; Bhargava, Suresh K;, *<A comparison study on carbon dioxide reforming of methane over Ni catalysts supported on mesoporous SBA 15 MCM 41 KIT 6 and Al2O3.pdf>*, in *Chemeca 2013*. 2013, Centre for Advanced Materials and Industrial Chemistry, School of Applied Sciences, RMIT University, Melbourne, VIC 3001, Australia, email: mohamadhassan.amin@rmit.edu.au: Australia. p. 543-548.

157. Samain, L., et al., *Structural analysis of highly porous γ-Al2O3.* Journal of Solid State Chemistry, 2014. **217**(0): p. 1-8.

158. Lu*, S.W.a.G.Q.M., *<A Comprehensive Study on Carbon Dioxide Reforming of Methane over Ni γ Al2O3 Catalysts.pdf>.* 1999.

159. Brungs, A., et al., *Dry reforming of methane to synthesis gas over supported molybdenum carbide catalysts.* Catalysis Letters, 2000. **70**(3-4): p. 117-122.

160.   Li, G., L. Hu, and J.M. Hill, *Comparison of reducibility and stability of alumina-supported Ni catalysts prepared by impregnation and co-precipitation.* Applied Catalysis A: General, 2006. **301**(1): p. 16-24.

161.   Wang, S. and G.Q. Lu, *Effects of promoters on catalytic activity and carbon deposition of Ni/γ-Al2O3 catalysts in CO2 reforming of CH4.* Journal of Chemical Technology & Biotechnology, 2000. **75**(7): p. 589-595.

162.   Wang, S. and G.Q. Lu, *Reforming of methane with carbon dioxide over Ni/Al2O3 catalysts: Effect of nickel precursor.* Applied Catalysis A: General, 1998. **169**(2): p. 271-280.

163.   Prashant Kumar, †,‡ Yanping Sun,†,§ and Raphael O. Idem†, *<Comparative Study of Ni-based Mixed Oxide Catalyst for Carbon Dioxide Reforming of Methane.pdf>.* 2008.

164.   Karl Sohlberg, † Stephen J. Pennycook,†,‡ and Sokrates T. Pantelides, *<Hydrogen and the Structure of the Transition Aluminas.pdf>.* 1999.

165.   Lu*, S.W.a.G.Q.M., *<Carbon Dioxide Reforming of Methane To Produce Synthesis Gas over Metal-Supported Catalysts State of the Art.pdf>.* 1995.

166.   Rahemi, N., et al., *Synthesis and physicochemical characterizations of Ni/Al2O3–ZrO2 nanocatalyst prepared via impregnation method and treated with non-thermal plasma for CO2 reforming of CH4.* Journal of Industrial and Engineering Chemistry, 2013. **19**(5): p. 1566-1576.

167.   Alipour, Z., M. Rezaei, and F. Meshkani, *Effect of alkaline earth promoters (MgO, CaO, and BaO) on the activity and coke formation of Ni catalysts supported on nanocrystalline Al2O3 in dry reforming of methane.* Journal of Industrial and Engineering Chemistry, 2014. **20**(5): p. 2858-2863.

168.   Wang, S. and G.Q. Lu, *Role of CeO2 in Ni/CeO2–Al2O3 catalysts for carbon dioxide reforming of methane.* Applied Catalysis B: Environmental, 1998. **19**(3–4): p. 267-277.

169.   Nimwattanakul, W., A. Luengnaruemitchai, and S. Jitkarnka, *Potential of Ni supported on clinoptilolite catalysts for carbon dioxide reforming of methane.* International Journal of Hydrogen Energy, 2006. **31**(1): p. 93-100.

170.   Khajeh Talkhoncheh, S. and M. Haghighi, *Syngas production via dry reforming of methane over Ni-based nanocatalyst over various supports of clinoptilolite, ceria and alumina.* Journal of Natural Gas Science and Engineering, 2015. **23**(0): p. 16-25.

171.   Al-Fatesh, A.S.A. and A.H. Fakeeha, *Reduction of green house gases by dry reforming: Effect of support.* Research Journal of Chemistry and Environment, 2011. **15**(2): p. 259-268.

172.   Chen, Y.-g., et al., *Noble metal promoted Ni0.03Mg0.97O solid solution catalysts for the reforming of CH4 with CO2.* Catalysis Letters, 1996. **39**(1-2): p. 91-95.

173.   Chubb, T.A., *Characteristics of CO2   CH4 reforming-methanation cycle relevant to the solchem thermochemical power system.* Solar Energy, 1980. **24**(4): p. 341-345.

174.   Liu, D., et al., *Carbon dioxide reforming of methane over nickel-grafted SBA-15 and MCM-41 catalysts.* Catalysis Today, 2009. **148**(3–4): p. 243-250.

175.   Guo, Y.H., C. Xia, and B.S. Liu, *Catalytic properties and stability of cubic mesoporous LaxNiyOz/KIT-6 catalysts for CO2 reforming of CH4.* Chemical Engineering Journal, 2014. **237**(0): p. 421-429.

176.   Joyner, R.W., *Principles of Catalyst Development by James T. Richardson. Plenum Press, New York 1989, xv, 288 pp., bound, US$ 59,40.—ISBN 0-306-43162-9 [163].* Advanced Materials, 1991. **3**(3): p. 170-171.

177.   Katsutoshi Nagaoka, M.O., Ken-ichi Aika, *<Titania supported ruthenium as a coking-resistant catalyst for high pressure dry reforming of methane.pdf>.* 2001

178.   Miyazawa, T., et al., *Catalytic performance of supported Ni catalysts in partial oxidation and steam reforming of tar derived from the pyrolysis of wood biomass.* Catalysis Today, 2006. **115**(1–4): p. 254-262.

179.   Wei, J.M., et al., *CO2 reforming of CH4 over Ni supported on nano-ZrO2(I) - Comparison with conventional oxide supported nickel.* Chemical Journal of Chinese Universities-Chinese, 2002. **23**(1): p. 92-97.

180.   Wang, S. and G.Q. Lu, *Catalytic Activities and Coking Characteristics of Oxides-Supported Ni Catalysts for CH4 Reforming with Carbon Dioxide.* Energy & Fuels, 1998. **12**(2): p. 248-256.

181.   Sarusi, I., et al., *CO2 reforming of CH4 on doped Rh/Al2O3 catalysts.* Catalysis Today, 2011. **171**(1): p. 132-139.

182.   Yokota, S., K. Okumura, and M. Niwa, *Support Effect of Metal Oxide on Rh Catalysts in the CH4-CO2 Reforming Reaction.* Catalysis Letters, 2002. **84**(1-2): p. 131-134.

183.   Kim, Y.H., et al., *Selective CO removal in a H2-rich stream over supported Ru catalysts for the polymer electrolyte membrane fuel cell (PEMFC).* Applied Catalysis A: General, 2009. **366**(2): p. 363-369.

184.   Vázquez-Zavala, A., et al., *Characterization of structure and catalytic activity of Pt–Sn catalysts supported in Al2O3, SiO2 and TiO2.* Applied Surface Science, 1998. **136**(1–2): p. 62-72.

185.   Nakagawa, K., et al., *Effect of support on the conversion of methane to synthesis gas over supported iridium catalysts.* Catalysis Letters, 1998. **51**(3-4): p. 163-167.

186.   Efstathiou, A.M., et al., *Reforming of Methane with Carbon Dioxide to Synthesis Gas over Supported Rhodium Catalysts: II. A Steady-State Tracing Analysis: Mechanistic Aspects of the Carbon and Oxygen Reaction Pathways to Form CO.* Journal of Catalysis, 1996. **158**(1): p. 64-75.

187. Xu, G., et al., *Studies of reforming natural gas with carbon dioxide to produce synthesis gas: X. The role of CeO2 and MgO promoters.* Journal of Molecular Catalysis A: Chemical, 1999. **147**(1–2): p. 47-54.

188. G. Leendert Bezemer, J.H.B., † Herman P. C. E. Kuipers,‡ Heiko Oosterbeek,‡ Johannes E. Holewijn,‡ Xiaoding Xu,§ Freek Kapteijn,§ A. Jos van Dillen,† and Krijn P. de Jong*,†, *<Cobalt Particle Size Effects in the Fischer-Tropsch Reaction Studied with Carbon Nanofiber Supported Catalysts.pdf>.* 2005.

189. Yu, M., et al., *The promoting role of Ag in Ni-CeO2 catalyzed CH4-CO2 dry reforming reaction.* Applied Catalysis B: Environmental, 2015. **165**(0): p. 43-56.

190. Al-Fatesh, A.S.A., A.H. Fakeeha, and A.E. Abasaeed, *Effects of Selected Promoters on Ni/Y-Al2O3 Catalyst Performance in Methane Dry Reforming.* Chinese Journal of Catalysis, 2011. **32**(9–10): p. 1604-1609.

191. Paksoy, A.I., B.S. Caglayan, and A.E. Aksoylu, *A study on characterization and methane dry reforming performance of Co–Ce/ZrO2 catalyst.* Applied Catalysis B: Environmental, 2015. **168–169**(0): p. 164-174.

192. Mattos, L.V., et al., *Partial oxidation and CO2 reforming of methane on Pt/Al2O3, Pt/ZrO2, and Pt/Ce–ZrO2 catalysts.* Fuel Processing Technology, 2003. **83**(1–3): p. 147-161.

193. Therdthianwong, S., C. Siangchin, and A. Therdthianwong, *Improvement of coke resistance of Ni/Al2O3 catalyst in CH4/CO2 reforming by ZrO2 addition.* Fuel Processing Technology, 2008. **89**(2): p. 160-168.

194. Valderrama, G., et al., *Dry reforming of methane over Ni perovskite type oxides.* Catalysis Today, 2005. **107–108**(0): p. 785-791.

195. Yang, E.-h., et al., *The effect of promoters in La0.9M0.1Ni0.5Fe0.5O3 (M = Sr, Ca) perovskite catalysts on dry reforming of methane.* Fuel Processing Technology, 2015. **134**(0): p. 404-413.

196. Moradi, G.R., M. Rahmanzadeh, and F. Khosravian, *The effects of partial substitution of Ni by Zn in LaNiO3 perovskite catalyst for methane dry reforming.* Journal of CO2 Utilization, 2014. **6**(0): p. 7-11.

197. Cheng, Z., et al., *Effects of promoters and preparation procedures on reforming of methane with carbon dioxide over Ni/Al2O3 catalyst.* Catalysis Today, 1996. **30**(1–3): p. 147-155.

198. Borowiecki, T., et al., *Studies of potassium-promoted nickel catalysts for methane steam reforming: Effect of surface potassium location.* Applied Surface Science, 2014. **300**(0): p. 191-200.

199. Borowiecki, T., et al., *The influence of promoters on the coking rate of nickel catalysts in the steam reforming of hydrocarbons*, in *Studies in Surface Science and Catalysis*, D.S.F.F.A.V. A. Parmaliana and F. Arena, Editors. 1998, Elsevier. p. 711-716.

200. Znak, L. and J. Zieliński, *The effect of potassium on Ni/Al2O3 catalyst in relation to CO/H2 reaction.* Applied Catalysis A: General, 2012. **413–414**(0): p. 132-139.

201. Lavoie, J.-M., *Review on dry reforming of methane, a potentially more environmentally-friendly approach to the increasing natural gas exploitation.* Frontiers in Chemistry, 2014. **2**: p. 81.

202. Mortensen, P.M. and I. Dybkjær, *Industrial scale experience on steam reforming of CO2-rich gas.* Applied Catalysis A: General, 2015. **495**(0): p. 141-151.

203. Pereira, A.L.C., et al., *A comparison between the precipitation and impregnation methods for water gas shift catalysts.* Journal of Molecular Catalysis A: Chemical, 2008. **281**(1-2): p. 66-72.

204. Zhang, G., et al., *Effects of preparation methods on the properties of cobalt/carbon catalyst for methane reforming with carbon dioxide to syngas.* Journal of Industrial and Engineering Chemistry, 2014. **20**(4): p. 1677-1683.

205. Osawa, T., et al., *Studies of the preparation method of ceria-promoted nickel catalyst for carbon dioxide reforming of methane.* Applied Catalysis A: General, 2014. **474**(0): p. 100-106.

206. Tsubaki, N., et al., *A new method of bimodal support preparation and its application in Fischer–Tropsch synthesis.* Catalysis Communications, 2001. **2**(10): p. 311-315.

207. Vergunst, T., F. Kapteijn, and J.A. Moulijn, *Monolithic catalysts — non-uniform active phase distribution by impregnation.* Applied Catalysis A: General, 2001. **213**(2): p. 179-187.

208. Zhuang, Y.Q., M. Claeys, and E. van Steen, *Novel synthesis route for egg-shell, egg-white and egg-yolk type of cobalt on silica catalysts.* Applied Catalysis A: General, 2006. **301**(1): p. 138-142.

209. Soled, S., et al., *Control of Metal Dispersion and Structure by Changes in the Solid-State Chemistry of Supported Cobalt Fischer–Tropsch Catalysts.* Topics in Catalysis, 2003. **26**(1-4): p. 101-109.

210. Ren, H.-P., et al., *High-performance Ni–SiO2 for pressurized carbon dioxide reforming of methane.* International Journal of Hydrogen Energy, 2014. **39**(22): p. 11592-11605.

211. Albarazi, A., M.E. Gálvez, and P. Da Costa, *Synthesis strategies of ceria–zirconia doped Ni/SBA-15 catalysts for methane dry reforming.* Catalysis Communications, 2015. **59**(0): p. 108-112.

212. Campanati, M., G. Fornasari, and A. Vaccari, *Fundamentals in the preparation of heterogeneous catalysts.* Catalysis Today, 2003. **77**(4): p. 299-314.

213. Wen, J. and J.E. Mark, *Precipitation of Silica-Titania Mixed-Oxide Fillers into Poly(Dimethylsiloxane) Networks.* Rubber Chemistry and Technology, 1994. **67**(5): p. 806-819.

214. Wen, J. and J.E. Mark, *Synthesis, structure, and properties of poly(dimethylsiloxane) networks reinforced by in situ-precipitated silica–titania, silica–zirconia, and silica–alumina mixed oxides.* Journal of Applied Polymer Science, 1995. **58**(7): p. 1135-1145.

215. Schüth, F., M. Hesse, and K.K. Unger, *Precipitation and Coprecipitation*, in *Handbook of Heterogeneous Catalysis*. 2008, Wiley-VCH Verlag GmbH & Co. KGaA.

216. Vos, B., E. Poels, and A. Bliek, *Impact of Calcination Conditions on the Structure of Alumina-Supported Nickel Particles.* Journal of Catalysis, 2001. **198**(1): p. 77-88.

217. Cavani, F., F. Trifirò, and A. Vaccari, *Hydrotalcite-type anionic clays: Preparation, properties and applications.* Catalysis Today, 1991. **11**(2): p. 173-301.

218. Martínez, R., et al., *CO2 reforming of methane over coprecipitated Ni–Al catalysts modified with lanthanum.* Applied Catalysis A: General, 2004. **274**(1–2): p. 139-149.

219. Benrabaa, R., et al., *Structure, reactivity and catalytic properties of nanoparticles of nickel ferrite in the dry reforming of methane.* Catalysis Today, 2013. **203**(0): p. 188-195.

220. Pinna, F., *Supported metal catalysts preparation.* Catalysis Today, 1998. **41**(1–3): p. 129-137.

221. Zanganeh, R., M. Rezaei, and A. Zamaniyan, *Preparation of nanocrystalline NiO–MgO solid solution powders as catalyst for methane reforming with carbon dioxide: Effect of preparation conditions.* Advanced Powder Technology, 2014. **25**(3): p. 1111-1117.

222. Bao, Z., et al., *Highly active and stable Ni-based bimodal pore catalyst for dry reforming of methane.* Applied Catalysis A: General, 2015. **491**(0): p. 116-126.

223. Behrens, M., *Coprecipitation: An excellent tool for the synthesis of supported metal catalysts – From the understanding of the well known recipes to new materials.* Catalysis Today, 2015. **246**(0): p. 46-54.

224. Cauqui, M.A. and J.M. Rodríguez-Izquierdo, *Application of the sol-gel methods to catalyst preparation.* Journal of Non-Crystalline Solids, 1992. **147–148**(0): p. 724-738.

225. Volovych, I., *<Sol gel processes in catalysis catalyst synthesis application recycling and combination to tandem reactions in microemulsions.pdf>*. 2014.

226. Zhang, Y., et al., *Preparation of titania-based catalysts for formaldehyde photocatalytic oxidation from TiCl4 by the sol–gel method.* Catalysis Today, 2001. **68**(1–3): p. 89-95.

227. Naeem, M.A., et al., *Hydrogen production from methane dry reforming over nickel-based nanocatalysts using surfactant-assisted or polyol method.* International Journal of Hydrogen Energy, 2014. **39**(30): p. 17009-17023.

228. Zhang, X., et al., *Carbon dioxide reforming of methane over Ni nanoparticles incorporated into mesoporous amorphous ZrO2 matrix.* Fuel, 2015. **147**(0): p. 243-252.

229. Kambolis, A., et al., *Ni/CeO2-ZrO2 catalysts for the dry reforming of methane.* Applied Catalysis A: General, 2010. **377**(1–2): p. 16-26.

230. Juan-Juan, J., M.C. Román-Martínez, and M.J. Illán-Gómez, *Effect of potassium content in the activity of K-promoted Ni/Al2O3 catalysts for the dry reforming of methane.* Applied Catalysis A: General, 2006. **301**(1): p. 9-15.

231. Micromeritics, *Automated Catalyst Characterization System AutoChem 2920*. 2014, Micromeritics Instrument Corporation 2006-2014. All rights reserved.

232. Castro Luna, A.E. and M.E. Iriarte, *Carbon dioxide reforming of methane over a metal modified Ni-Al2O3 catalyst.* Applied Catalysis A: General, 2008. **343**(1–2): p. 10-15.

233. Laosiripojana, N., W. Sutthisripok, and S. Assabumrungrat, *Synthesis gas production from dry reforming of methane over CeO2 doped Ni/Al2O3: Influence of the doping ceria on the resistance toward carbon formation.* Chemical Engineering Journal, 2005. **112**(1–3): p. 13-22.

234. Djaidja, A., et al., *Characterization and activity in dry reforming of methane on NiMg/Al and Ni/MgO catalysts.* Catalysis Today, 2006. **113**(3–4): p. 194-200.

235. Therdthianwong, S., et al., *Synthesis gas production from dry reforming of methane over Ni/Al2O3 stabilized by ZrO2.* International Journal of Hydrogen Energy, 2008. **33**(3): p. 991-999.

236. Kathiraser, Y., et al., *Kinetic and mechanistic aspects for CO2 reforming of methane over Ni based catalysts.* Chemical Engineering Journal, 2015.

237. Navarro, R.M., et al., *Hydrogen production by oxidative reforming of hexadecane over Ni and Pt catalysts supported on Ce/La-doped Al2O3.* Applied Catalysis A: General, 2006. **297**(1): p. 60-72.

238. Özkara-Aydınoğlu, Ş., *Thermodynamic equilibrium analysis of combined carbon dioxide reforming with steam reforming of methane to synthesis gas.* International Journal of Hydrogen Energy, 2010. **35**(23): p. 12821-12828.

239. Oyama, S.T., et al., *Dry reforming of methane has no future for hydrogen production: Comparison with steam reforming at high pressure in standard and membrane reactors.* International Journal of Hydrogen Energy, 2012. **37**(13): p. 10444-10450.

240. Bradford, M.C.J. and M.A. Vannice, *CO2Reforming of CH4over Supported Ru Catalysts.* Journal of Catalysis, 1999. **183**(1): p. 69-75.

241. Iyer, M.V., et al., *Kinetic Modeling for Methane Reforming with Carbon Dioxide over a Mixed-Metal Carbide Catalyst.* Industrial & Engineering Chemistry Research, 2003. **42**(12): p. 2712-2721.

242. Shamsi, A. and C.D. Johnson, *Effect of pressure on the carbon deposition route in CO2 reforming of 13CH4.* Catalysis Today, 2003. **84**(1–2): p. 17-25.

243. Tsipouriari, V.A., et al., *Reforming of methane with carbon dioxide to synthesis gas over supported Rh catalysts.* Catalysis Today, 1994. **21**(2–3): p. 579-587.

244. Istadi1), N.A.S.A., *<Co Generation of C2 Hydrocarbons and Synthesis Gases from Methane and Carbon Dioxide a Thermodynamic Analysis.pdf>.* 2005.

245. Wang, S., G.Q. Lu, and G.J. Millar, *Carbon Dioxide Reforming of Methane To Produce Synthesis Gas over Metal-Supported Catalysts: State of the Art.* Energy & Fuels, 1996. **10**(4): p. 896-904.

246. Khalesi, A., H.R. Arandiyan, and M. Parvari, *Effects of Lanthanum Substitution by Strontium and Calcium in La-Ni-Al Perovskite Oxides in Dry Reforming of Methane.* Chinese Journal of Catalysis, 2008. **29**(10): p. 960-968.

247. Wisniewski, M., A. Boréave, and P. Gélin, *Catalytic CO2 reforming of methane over Ir/Ce0.9Gd0.1O2−x.* Catalysis Communications, 2005. **6**(9): p. 596-600.

248. Li Yanbing, J.B.a.X.R., *<Carbon dioxide reforming of methane with a free energy minimization approach.pdf>.* 2006.

249. Istadi, N.A.S.A., *Cogeneration of C2 Hydrocarbons and Synthesis Gases from Methane and Carbon Dioxide: A Thermodynamic Analysis.* J. Nat. Gas Chem., 14 (2005), pp. 140–150, 2005.

250. Takano, A., T. Tagawa, and S. Goto, *Carbon Dioxide Reforming of Methane on Supported Nickel Catalysts.* JOURNAL OF CHEMICAL ENGINEERING OF JAPAN, 1994. **27**(6): p. 727-731.

251. Seshan, K., J.H. Bitter, and J.A. Lercher, *Design of stable catalysts for methane — carbon dioxide reforming*, in *Studies in Surface Science and Catalysis*, T.S.R.P. Rao and G.M. Dhar, Editors. 1998, Elsevier. p. 187-191.

252. Choudhary, V., et al., *Carbon-free dry reforming of methane to syngas over NdCoO3 perovskite-type mixed metal oxide catalyst.* Catalysis Letters, 2005. **100**(3-4): p. 271-276.

253. John B. Claridge, M.L.H.G., Shik Chi Tsang, *<A study of carbon deposition on catalysts during the partial oxidation of methane to synthesis gas.pdf>.* 1993.

254. Noronha, F.B., et al., *Catalytic Performance of Pt/ZrO2 and Pt/Ce-ZrO2 Catalysts on CO2 Reforming of CH4 Coupled with Steam Reforming or Under High Pressure.* Catalysis Letters, 2003. **90**(1-2): p. 13-21.

255. Song, S.-H., et al., *The influence of calcination temperature on catalytic activities in a Co based catalyst for CO2 dry reforming.* Korean Journal of Chemical Engineering, 2014. **31**(2): p. 224-229.

256. Wang, X., et al., *Thermodynamic analysis of glycerol dry reforming for hydrogen and synthesis gas production.* Fuel, 2009. **88**(11): p. 2148-2153.

257. Ki-Dong Ko*, J.K.L., Dalkeun Park t and See Hee Shin*, *<KINETICS OF STEAM REFORMING OVER A Ni ALUMINA CATALYST.pdf>.* 1995.

258. Akpan, E., et al., *Kinetics, experimental and reactor modeling studies of the carbon dioxide reforming of methane (CDRM) over a new – catalyst in a packed bed tubular reactor.* Chemical Engineering Science, 2007. **62**(15): p. 4012-4024.

259. Becerra, A., M. Iriarte, and A. Castro Luna, *Catalytic activity of a nickel on alumina catalyst in the CO2 reforming of methane.* Reaction Kinetics and Catalysis Letters, 2003. **79**(1): p. 119-125.